

Energy-scales convergence for optimal and robust quantum transport in photosynthetic complexes

M. Mohseni,¹ A. Shabani,² S. Lloyd,³ and H. Rabitz²

¹*Center for Excitonics, Research Laboratory of Electronics,
Massachusetts Institute of Technology, Cambridge, MA 02139*

²*Department of Chemistry, Princeton University, Princeton, New Jersey 08544*

³*Department of Mechanical Engineering, Massachusetts Institute of Technology, Cambridge, MA 02139*

Underlying physical principles for the high efficiency of excitation energy transfer in light-harvesting complexes are not fully understood. Notably, the degree of robustness of these systems for transporting energy is not known considering their realistic interactions with vibrational and radiative environments within the surrounding solvent and scaffold proteins. In this work, we employ an efficient technique to estimate energy transfer efficiency of such complex excitonic systems. We observe that the dynamics of the Fenna-Matthews-Olson (FMO) complex leads to optimal and robust energy transport due to a convergence of energy scales among all important internal and external parameters. In particular, we show that the FMO energy transfer efficiency is optimum and stable with respect to the relevant parameters of environmental interactions and Frenkel-exciton Hamiltonian including reorganization energy λ , bath frequency cutoff γ , temperature T , bath spatial correlations, initial excitations, dissipation rate, trapping rate, disorders, and dipole moments orientations. We identify the ratio of $\lambda T/\gamma g$ as a single key parameter governing quantum transport efficiency, where g is the average excitonic energy gap.

PACS numbers:

I. INTRODUCTION

Life on the earth has been solar-powered via the mechanism of photosynthesis for four billions years [1]. Photosynthetic antenna complexes have evolved to harvest the sun's energy and efficiently transport it to reaction centers where it is stored as biochemical energy. The first few steps in photosynthesis represent highly sophisticated energy capture and transfer processes, as in an efficient solar cell. Specialized pigments in the antenna complexes absorb energy from sunlight, creating electron-hole pairs known as *excitons*. The excitons then travel to reaction centers where their energy is converted and stored as chemical energy. The key feature for the success of photosynthesis is the high efficiency of exciton transport – as high as 99% in certain bacterial systems [2]. Thus, photosynthetic complexes provide an excellent model for designing efficient artificial excitonic devices. Unfortunately, the fundamental structural and dynamical processes contributing to such efficient migration of excitons are not fully understood.

During the last two decades, many spectroscopic observations for extended excitation states over multiple chromophores within light-harvesting complexes have been reported [3, 4]. These results support the quantum mechanically delocalized nature of excitations in spatial coordinate. A variety of theoretical models have been proposed to capture the nature of delocalized quantum coherence effects in excitonic energy transfer [5–16]. These models employ various generalizations of Förster energy transport [17, 18] and Redfield theory [19] in different perturbative limits. Specific effects of quantum coherence in multichromophoric donor to acceptor energy transfer rates were also studied in details [15]. Recent advances in multidimensional electronic spectroscopy provide evidence that long-lived quantum dynamical coherence can exist in exciton basis [20–28]. These experiments reported oscillatory coherences that were observed to last around 500 *fs*, which is on the same order as the transport time-scale.

The observations were made at cryogenic and physiological temperatures for several light-harvesting complexes including the FMO complex of green sulfur bacteria [20, 26], reaction center (RC) of purple bacteria [21], light-harvesting complex II of higher plants [22], conjugated polymers [24], and marine algae [25]. It was specifically suggested by Engel and Fleming that quantum dynamical interference effects might explain exceptionally high energy transfer efficiency of light-harvesting systems [20]. This conjecture has led to vigorous theoretical efforts to try to understand the role of coherence in excitonic transport [29–45]. Despite considerable progress in experiment and theory, it is still unknown how quantum coherence can be preserved in such unusually warm, complex and wet conditions. Moreover, it is not yet fully understood if quantum interference effects, in either spatial or energy coordinates, are contributing to efficiency of these systems. More importantly, it is not known how robust and optimal are these complexes with respect to variations in the coherent system evolution and/or environmental parameters.

Reference [29] demonstrated that an effective collaboration between coherent quantum evolution and environmental fluctuations could enhance photosynthetic energy transfer efficiency (ETE). This work was based on a quantum trajectory picture in site basis [29], within the Born-Markov and secular approximations which guarantee complete positivity of the excitonic dynamics [46]. However, due to the perturbative approximation used in this model, it was impossible to explore the optimality of energy transfer efficiency in the relevant regimes of intermediate system-bath coupling strength. Moreover, due to secular approximation, the coherence and population transfers are essentially decoupled. In order to avoid such problems subsequent studies relied on non-perturbative Haken-Strobl method [6] to be able to explore a wider range of environmental interactions in the context of a (pure-dephasing) classical white-noise model at infinite temperature. These model studies illustrate optimal ranges of

dephasing-assisted excitation transfer [31–33]. In the optimal regime, an appropriate level of environmental fluctuations can wash out the quantum localization effects at the equilibrium state, when they are not too strong to lead to quantum Zeno effect [31]. These models, however, are by construction inadequate to capture the role of quantum interplay of system evolution with non-equilibrium dynamics of bath within realistic non-perturbative and non-Markovian regimes [35].

Recently Ishizaki and Fleming developed a general approach for studying excitation energy transfer in multichromophoric systems based on a hierarchy of coupled master equations [36]. Using this Hierarchy Equation of Motion (HEOM), first introduced by Kubo and Tanimura [47], quantum coherent beating in the FMO protein at physiological temperature was investigated theoretically [37]. Although, HEOM can be in principle applied to all the different regimes of environmental interactions as a general benchmark, the requires computational resources significantly increase with the size of the system, the bath correlation time-scale, and within low temperature regimes. Thus, a number of alternative or complementary techniques for simulation of open quantum dynamics have been recently proposed [48–54]. We have recently shown that the second-order time-convolution (TC2) master equation can be used to efficiently estimate ETE in large complex excitonic systems interacting with bosonic environments in the *intermediate* regimes [55]. This method is based on the Cao’s earlier work on the generalized Bloch-Redfield master equations [48]. In Ref. [55] we examined the TC2 master equation reliability beyond extreme Markovian and perturbative limits.

In this paper, we observe that the FMO pigment-protein complex is optimal and robust with respect to all the estimated parameters of system and environmental interactions, within the TC2 master equation evolution for either of Lorentzian or Ohmic spectral densities of the environment. The paper contains the following main results:

- We show that efficient and fault-tolerant energy transport occurs when the FMO internal parameters are in tune with environmental parameters leading to a collaborative interplay of the coherent free Hamiltonian evolution and incoherent effects due to environment.
- We comprehensively study the effects of reorganization energy λ , bath frequency cutoff γ , temperature T , positive and negative spatial correlations, loss, and trapping mechanisms on the energy transfer efficiency (ETE) landscapes. We show that ETE is optimal for the physiologically estimated value of these parameters, and is robust over a wide range of variations in these parameters.
- We demonstrate that a convergence of time/energy scales for the relevant internal and environmental parameters of FMO complex facilitates efficient energy transport. For an excitonic system with average energy gap g , we observe that a single effective parameter $\Lambda = \lambda T / \gamma g$ governs the behavior of quantum transport dynamics. Small values $\Lambda \ll 1$ give rise to weak localization and low efficiency. Intermediate values

$\Lambda \approx 1$ correspond to the optimal energy transfer. Large values $\Lambda \gg 1$ give rise to strong localization and low efficiency.

- We observe that positive/negative spatial correlations essentially renormalize the reorganization energy to effective lower/higher values. The positive bath correlations can significantly enhance ETE at the regime of large λ by inducing symmetries in the effective phonon-exciton Hamiltonian protecting the transport against strong dynamical disorder. In the intermediate values of system-bath coupling, the spatial correlations can enhance the robustness of transport efficiency. However, at the very small values of reorganization energy, they have an adversarial effect by diminishing useful but very weak bath fluctuations.
- To explore the dynamical role of coherent system evolution, we examine whether or not the spatial structure of the FMO complex plays any important role in its performance. We find that the FMO compact structure is instrumental for supporting high efficiency. Moreover, we directly demonstrate that the FMO performance is robust to variations in its geometrical parameters considering its rich internal parameter space. Specifically, the efficiency of FMO is robust to variations in the orientations of dipole moments and site energies due to its compact structure.
- Finally, we discuss possibility of a so-called *Goldilocks principle* in the quantum regime that could explain the convergence of time-scales in FMO complex and other light-harvesting systems, with respect to internal parameters and environmental interactions. The Goldilocks principle for complex systems postulates a ‘just right’ level of complexity – too little complexity compromises function, while too much complexity compromises robustness. Convergence of timescales increases complexity by allowing different quantum processes to interact strongly with each other. These interactions have the potential either to reduce or to increase efficiency and robustness. For the FMO complex and other simplified small-size light-harvesting systems, we show that the convergence of timescales effectively acts to increase both efficiency and robustness. Such a fundamental principle could also serve a key guiding rule for designing optimal materials to achieve exceptional quantum transport performance in realistic environments.

The organization of the paper is as follows: section II reviews the TC2 master equation that we employ to efficiently simulate energy transport in multichromophoric systems in low excitation regimes [55]. In the section III, the efficiency and sensitivity of the FMO is studied with respect to the environmental parameters including reorganization energy, bath cutoff frequency, temperature, bath spatial correlations, and trapping. In section IV, we consider the dependence of ETE on variations in temporal and geometrical factors of the trapping mechanism for FMO. The role of initial excitonic states is investigated in the section V. In the section VI, we study the robustness of ETE in presence of disorder in the FMO internal

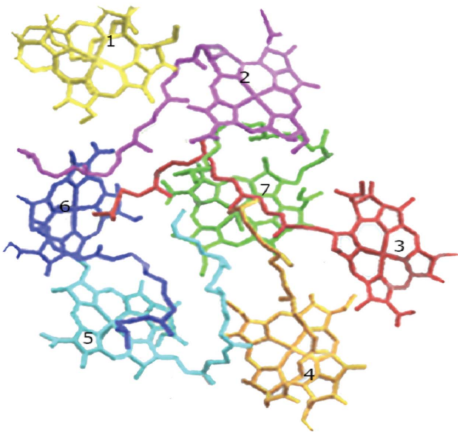


FIG. 1: The disordered structure of the Fenna-Matthews-Olson (FMO) complex: It is a trimer consisting of three identical monomers each formed from seven BChls embedded in a scaffold protein. The FMO complex acts as an energy transfer channel in green sulphur bacteria guiding excitons from the light-harvesting antenna complex, in the proximity of BChls 1 and 6, to the reaction center which is in the proximity of BChls 3 and 4.

structure parameterized by site energies, inter-chlorophyll distances, and dipole moment orientations. Some complementary materials for FMO complex are presented in the appendices on the FMO structural data and ETE in the presence of an Ohmic bath.

II. THEORETICAL MODEL OF THE FMO COMPLEX

To explore optimality and robustness of natural or artificial light-harvesting complexes we compute the energy transfer efficiency landscape as a function of the independent degrees of freedom of the pigment-protein complex including thermal and vibrational environments. This imposes two fundamental obstacles to developing analytical and computational approaches that can be employed in this context. The first problem is the fact that these systems are complex and contain a significant number of important physical variables. These independent parameters and their dynamical interplay have to be fully explored as they could play a major role in the energy transfer dynamics within these complexes. The second problem is that the common theoretical models, including Förster, Haken-Strobl, Redfield or Lindblad theory, are based on simplifying perturbative and/or Markovian assumptions that are inadequate by construction [35]. This second problem exists even if the estimated parameters of the system or system-bath couplings are rather weak and when bath has little or no memory. The difficulty is that for studying the optimality or robustness of these complexes one has to fully explore both topology and geometry of energy transfer efficiency landscape outside of the known values of a given pigment-protein complex [56]. The combination of these two problems indicates that such study will be practically intractable with current state of the art simulation techniques such as HEOM [37], which, while

accurate, are computationally highly expensive. Recently, we have derived the well-known time nonlocal master equation TC2 without making the usual weak system-bath coupling assumption. In this section, we summarize the main relevant definitions and equations of that approach. For more technical details we refer the readers to Ref. [55].

The dynamics of a multichromophoric system interacting with surrounding scaffold protein and solvent can be understood by starting from a general time evolution formulation of open quantum systems. The total system-bath Hamiltonian can be expressed as

$$H_{total} = H_S + H_{ph} + H_{S-ph} \quad (1)$$

where

$$\begin{aligned} H_S &= \sum_{j,k} \epsilon_j |j\rangle\langle j| + J_{jk} |j\rangle\langle k|, \\ H_{ph} &= \sum_{j,\xi} \hbar\omega_\xi (p_{j,\xi}^2 + q_{j,\xi}^2)/2, \\ H_{S-ph} &= \sum_j S_j B_j. \end{aligned}$$

The phonon bath is modeled as a set of harmonic oscillators [57]. Here $|j\rangle$ denotes an excitation state in a chromophore spatially located at site j . The diagonal site energies are denoted by ϵ_j that include reorganization energy shifts $\lambda_j = \sum_\xi \hbar\omega_\xi d_{j,\xi}^2/2$ due to interactions with a phonon bath; $d_{j,\xi}$ is the dimensionless displacement of the (j, ξ) th phonon mode from its equilibrium configuration. The strengths of dipole-dipole interactions between chromophores in different sites are represented by J_{jk} . The operators $S_i = |i\rangle\langle i|$ and $B_j = -\sum_\xi \hbar\omega_\xi d_{j,\xi} q_{j,\xi}$ are system and bath operators. Here, we assume that each site is linearly interacting with a separate phonon bath. The overall dynamics of the system can be expressed by a time-nonlocal master equation, e.g., TC2, [55] as:

$$\begin{aligned} \frac{\partial}{\partial t} \rho(t) &= \mathcal{L}_S \rho(t) + \mathcal{L}_{e-h} \rho(t) \\ &- \sum_j [S_j, \frac{1}{\hbar^2} \int_0^t C_j(t-t') e^{\mathcal{L}_S(t-t')} S_j \rho(t') dt' - h.c.] \end{aligned} \quad (2)$$

where $C_j(t-t_1) = \langle \tilde{B}_j(t) \tilde{B}_j(t_1) \rangle$ represent the bath correlation function, and the Liouvillian superoperators \mathcal{L}_S , \mathcal{L}_{ph} and \mathcal{L}_{S-ph} associated to H_S , H_{ph} and H_{S-ph} respectively. The term $\mathcal{L}_{e-h} = -\sum_j r_{loss}^j \{ |j\rangle\langle j|, \cdot \} - r_{trap} \{ |trap\rangle\langle trap|, \cdot \}$ captures two different competing electron-hole pair recombination processes that determine the energy transfer efficiency of light harvesting complexes. The first process is the loss due to dissipation to the environment at each site that happens within the time-scale of 1 ns. This inevitable adverse environmental effect guarantees that the energy transfer efficiency has a value less than one. The second process is the desired recombination process due to successful trapping.

The ETE is defined as accumulated probability of exciton being successfully trapped:

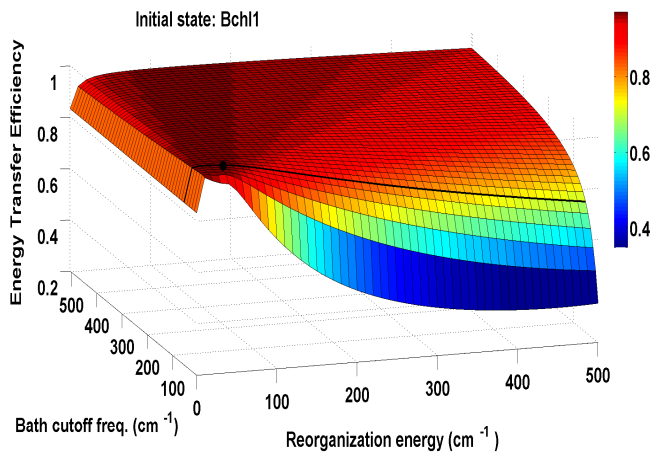


FIG. 2: The Energy transfer efficiency (ETE) of the Fenna-Matthews-Olson complex versus reorganization energy λ (as a measure of decoherence strength) and bath cutoff frequency γ (as a measure of non-Markovian character of the bath [65, 66]). The experimentally estimated values of $T = 298 \text{ }^\circ\text{K}$, $\lambda = 35 \text{ cm}^{-1}$, $\gamma = 50 - 166 \text{ cm}^{-1}$, $r_{trap}^{-1} = 1 \text{ ps}$ and $r_{loss}^{-1} = 1 \text{ ns}$ reside at an optimal and robust neighborhood of ETE. The FMO complex would act sub-optimally in the regimes of large γ and very small λ , or large λ and very small γ . In the intermediate values of λ/γ the phenomenon of environment-assisted quantum transport takes place. A top view of this plot in Fig. 3 indicates λ/γ is the parameter that governs efficiency at a fixed temperature.

$$\eta = 2r_{trap} \int_0^\infty \langle trap | \rho(t) | trap \rangle dt \quad (3)$$

The above performance function is biologically relevant and has been extensively used for a variety of light-harvesting complexes [9, 29, 55].

In this work, we mostly concentrate on the dynamics of the FMO pigment-protein complex of the bacterium *Chlorobium tepidum* [63] as a prototype for larger light-harvesting antenna complexes, Fig. 1. The structure of this pigment-protein complex was the first of light-harvesting complexes to be determined by x-ray crystallography [62]. The FMO structure consists of a trimer, formed by three identical monomers, each includes a closely packed assembly of seven BChl-a molecules. The FMO trimer guides excitation energy transfer between the chlorosome, the light-harvesting antennae of green sulfur bacteria, and the membrane-embedded type I reaction center (RC). In the following sections for our numerical simulations, unless specified otherwise, the environmental parameters for the FMO complex are chosen according to the experimentally or theoretically estimated values of reorganization energy 35 cm^{-1} , temperature $298 \text{ }^\circ\text{K}$, trapping rate of 1 ps , exciton lifetime of 1 ns , and zero spatial correlations. In the present simulations, we adopt the bath cutoff frequency of 50 cm^{-1} from the studies in Refs. [4, 72]. However we have repeated our simulations for another reported estimation of $\gamma = 166 \text{ cm}^{-1}$, Ref. [59], and we observed no significant difference in the behavior of ETE landscape. The diagonal and off-diagonal free

Hamiltonian parameters are given in appendix A, as functions of chromophoric distances, dipole moment angles and site energies. The trapping rate is treated as a free parameter in section IV. For most of this manuscript we assume an excitation initially localized at site 1. Similar results are obtained for other initializations such as localized state at site 6. We study the overall, best, and worst case scenarios of dependency on the initial states in the section V. In the next section, we use Eq. (3) to demonstrate efficiency and robustness of the FMO complex with respect to variations in reorganization energy, temporal correlations, temperature and spatial correlations.

III. OPTIMALITY AND ROBUSTNESS WITH RESPECT TO ENVIRONMENTAL PARAMETERS

We employ the time-nonlocal master equation presented above to efficiently estimate the energy transfer efficiency *landscape* as a function of various independent system and environmental degrees of freedom over a wide range of values. This efficient simulation allows us to examine comprehensively all relevant regimes of the multiparameter space for finding possible high efficient and robust neighborhoods. Only after such exhaustive study can one quantify the performance of any particular natural photosynthetic complexes. Moreover, such studies shed light on the maximum capabilities that can be achieved for optimal material design to engineer and characterize fault-tolerant artificial light-harvesting systems [60, 61] within a given rich system-environmental parameter space. The quantum efficiency of photosynthetic energy conversion can also be estimated by measuring the quantum requirements of ATP formation [2]. Thus, the overall robustness and optimality of a pigment-protein complex can also be experimentally explored, verified, or calibrated by varying the tunable parameters in the laboratory. For example, this can be achieved by changing ambient temperature and using diverse solvents with different dielectric properties [61].

In addition to our landscape study of ETE, we also examine the degree of optimality and robustness of the energy transfer by employing the the Euclidean norm of the gradient and Hessian matrix of the ETE function. The Euclidean norm of the ETE gradient at any parameters values p_1 and p_2 , $\|\nabla\eta(p_1, p_2)\|_2$, quantifies the degree of optimality. The gradient measure reveals the degree of local optimality in a surface manifold. Careful inspections of the room temperature plots for the ETE function versus various pairs of relevant parameters show a convex or concave manifold, thus gradient as a measure of local optimality suffices to measure global optimality. To examine the robustness, we compute the Hessian matrix norm $\|H(\eta(p_1, p_2))\|_2 = \|[\partial^2\eta/\partial p_i\partial p_j]\|_2$ ($i, j = 1, 2$) as the total measure of local curvature of the manifold. A smaller value of this norm corresponds to a flatter surface, thus a more robust process. We use a five-point stencil method to compute derivatives numerically.

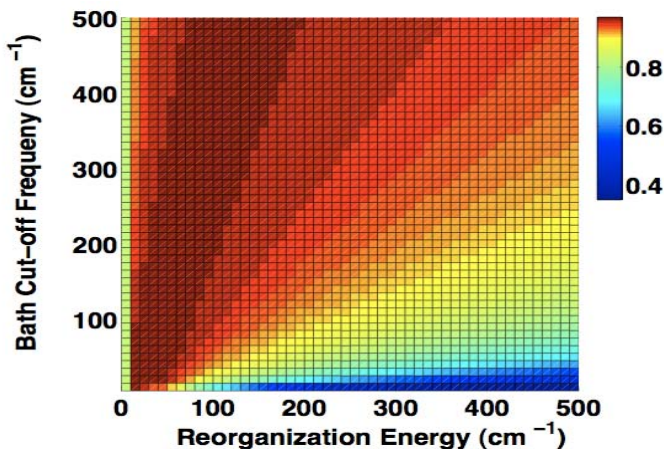


FIG. 3: Top view of ETE landscape illustrated in Fig. 2 indicating that the ratio of the reorganization energy over bath frequency cutoff can be considered as the parameter that governs the energy transfer efficiency at a fixed temperature. As we inspect this plot in an angular coordinate from the vertical axis, γ , toward the horizontal axis, λ , we can distinguish different regions of the ETE landscape that are separated by straight lines λ/γ . At very small decoherence rate, the FMO complex experiences weak localization due to static disorder. As we increase this ratio, an optimal region of ETE emerges that is induced by an appropriate level of interplay between environmental fluctuations and coherent evolution. At higher levels of this parameter, ETE drops significantly due to strong localization induced by dynamical disorder.

A. Reorganization energy and non-Markovianity

We first explore the variation of the FMO energy transfer efficiency versus reorganization energy and bath cutoff frequency using a Lorentzian spectral density, see Fig. 2. The reorganization energy, λ , is proportional to the squared value of the system-bath couplings, quantifying the decoherence strength. The bath cutoff frequency is the inverse of the bath coherence time-scale that captures the non-Markovian nature of the environment. That is, the non-Markovianity measure, defined as the information flow from the system to the phonon bath by Breuer et. al. [65], increases exponentially with decreasing bath cutoff frequency [66]. The ETE function has not been illustrated in Fig. 2 for bath cutoff frequency values less than $\gamma = 5 \text{ cm}^{-1}$, since according to our analysis in Ref. [55] the simulation errors of TC2 master equation may become significant in such highly non-Markovian regimes. It should be noted that in the regime of $\gamma > \beta^{-1}$ we apply low temperature corrections to the bath correlation function as explained in the next section.

The optimality and robustness of ETE for the FMO protein complex at the experimentally estimated values of $\lambda = 35 \text{ cm}^{-1}$ and $\gamma = 50 - 166 \text{ cm}^{-1}$ are evident in Fig. 2. An independent study on the optimality of ETE versus reorganization energy has been recently reported in Ref. [67]. It can be observed in Fig. 2 that the non-Markovianity of the bath can slightly increase ETE in the regimes of weak system-bath coupling. However, such slow bath behavior can significantly

decrease ETE when the system interacts strongly with it. The main question is how one can understand this phenomenon for all non-Markovian and Markovian regimes in the context of Environment-Assisted Quantum Transport (ENAQT), which was first investigated using simplified formalisms of the Lindblad (weak coupling and Markovian assumptions) [29] and Haken-Strobl (infinite temperature, pure-dephasing assumption) [30].

In this work, we report an underlying theory for environment-assisted quantum transport. The landscape in Fig. 2 shows a remarkable interplay of reorganization energies λ and bath frequency cutoff γ . The ETE takes values below unity if the FMO operates at the limit of very small λ and large γ . On the other limit, the FMO efficiency drops significantly when operating at large λ and very small γ . As we argue below these two regimes can be understood as manifestations of weak- and strong quantum localization, respectively.

A note on terminology: we use the terms weak and strong localization in analogue to the corresponding effects in bulk solid-state systems [68]. However, in contrast to solid state systems, here we are dealing with finite-size systems of few chromophores. In addition, it is important to note that because of the long-range nature of the dipolar force, the bulk versions of these chromophoric systems would not exhibit exponentially localized states. What is really being investigated here, then is a kind of *transient* localization which would eventually go away due to the long-range nature of the dipolar force and the small system size. If the destruction of transient localization takes longer than the exciton lifetime, however, then transient localization is just as adversarial to quantum transport efficiency as full localization. In this paper, when we refer to weak and strong localization, the reader should keep in mind that we are actually discussing weak and strong transient localization.

In order to fully explore the regimes of weak and strong localization and the various intermediate transitional regions, we illustrate a top view of Fig. 2 in Fig. 3. This plot immediately reveals that the regions of distinct energy transfer efficiencies at room temperature are governed by a parameter of the form λ/γ . For small and for large values of this parameter, the efficiency is low. The efficiency reaches its maximum for intermediate values of this parameter. In both strong and weak quantum localization limits the excitation will be spatially trapped in the regions typically far from reaction center and eventually dissipating to bath due to adversarial electron-hole recombination processes which occur on three order of magnitude slower time-scale. In the intermediate regime, the right amount of the interplay of quantum coherence and environmental fluctuations can facilitate an optimal energy transport in a robust fashion by various physical mechanisms including minimizing site energy mismatches, washing out potential destructive quantum interference effects, and enhancing the energy funneling by providing an appropriate vibrational energy sink.

The dependence of efficiency on λ/γ can be understood as follows. When the FMO complex interacts weakly with its environment the exciton migration is essentially dictated by the site energies and inter-pigment couplings. The spatial lo-

cations, Fig. 1, and dipole moments of BCHs do not show any obvious regular pattern. In the absence of environmental interactions, destructive interference effects due to such random configurations can cause weak localization over a few chromophores away from the trapping site. This phenomenon prevents successful delivery of the initial exciton to the reaction center and therefore leads to below unity efficiency of about 83% at $\lambda = 0$. Weak localization is amplified by lowering the temperature, a behavior observed in the simulations presented in the next section. By increasing the system-bath coupling strength, the adversarial interference effects of excitonic pathways are diminished in a fashion similar to observations reported in Refs. [29, 30, 32]. However, here it can be observed in Fig. 3 that for larger bath cutoff frequencies, a larger reorganization energy is required for ENAQT to occur.

We can understand these observations in terms of ENAQT by noting that the effective decoherence rate is given by λ/γ in the perturbative limit at a fixed temperature [46]. This ratio becomes smaller as we raise the γ therefore a stronger coupling λ is needed to guarantee the level of decoherence strength required for ENAQT. The overlap of a delocalized exciton wave function with the trap enables an almost complete, 98% quantum transport in the optimal range of λ/γ at the ambient temperature. As we increase the reorganization energy and bath coherence time-scale, the ETE starts to drop. In this regime, excitonic wave function again experiences localization as the environmental fluctuations change their role to play a strong adversarial effect on the quantum transport essentially as a source of strong dynamical disorder. The ETE landscape in Fig. 3, clearly has level sets that exhibit linear relationship with λ and γ . Indeed the ratio λ/γ , known as the Kubo number, is the parameter that governs Anderson localization transition in stochastic classical modeling of environmental interactions. [68–71]. In the fixed high-temperature limit of ETE illustrated in Fig. 3, one can observe that λ/γ is a determining parameter for transport efficiency in the regions beyond optimal ENAQT area. In the next section, we go beyond the Kubo number, by directly investigating the temperature dependent energy transfer dynamics, leading to a general governing parameter as $\lambda T/\gamma$.

A more quantitative study of the degree of optimality and robustness of the energy transfer as functions of system-bath coupling strength and bath memory is illustrated in Fig 4. The optimality is defined as Euclidean norm of the ETE function gradient $\|\nabla\eta(\lambda, \gamma)\|_2$ to locate the local maxima in the ETE landscape in Fig. 4. The robustness is defined by $\|H(\eta(\lambda, \gamma))\|_2$ to measure local curvature of the manifold. Note that the ETE gradient and Hessian matrix norms are indicated in a logarithmic scale, thus the global optimal point with zero derivative can not be explicitly highlighted in this representation. The experimentally estimated values for FMO are illustrated as black dots in each graph clearly located in an optimal and robust region. One remarkable feature is the fact that environmental parameters of FMO have almost the minimal reorganization energy and bath cutoff frequency among all the regions with simultaneous optimal and robust properties. This might be explained by the overall tendency in nature to minimize the amount of required work, that is, facilitating

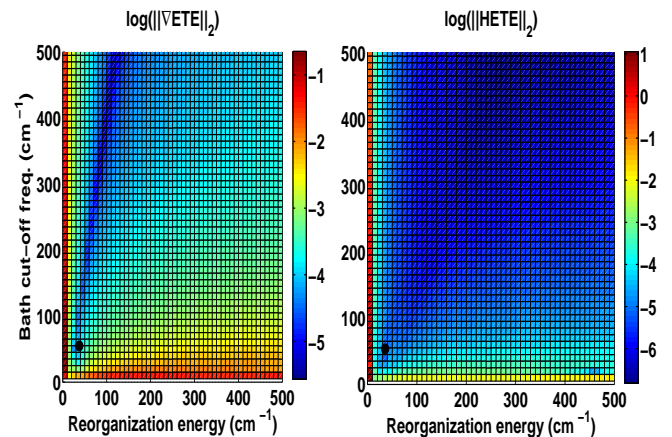


FIG. 4: This figure is a complement to Fig. 2. (Left) The degree of ETE optimality is quantified at different values of λ and γ by the gradient matrix norm of the ETE function. The dark blue points represent near optimal values. (Right) The degree of ETE robustness is quantified by the Euclidian norm of Hessian of the ETE. The dark blue points represent near robust points. The estimated FMO environmental values of $\lambda = 35\text{cm}^{-1}$ and $\gamma = 50\text{cm}^{-1}$, marked by black dots, are located on the corner of both robust and optimal region. This implies the FMO environmental conditions provide the minimal work required for facilitating optimal and robust energy transport by maintaining a rather weakly-coupled small scaffold protein.

an optimal and robust environmental platform for the FMO energy transport by preserving a rather small size scaffold protein that is weakly coupled.

The theoretical and experimental modeling of the environment surrounding the FMO complex suggests that the spectral density of the phonon bath modes can be expressed as a some of a few Lorentzian terms [57]. The spectral density function $J(\omega)$ determines the time correlation functions as:

$$\langle \tilde{B}(t)\tilde{B}(0) \rangle = \frac{1}{\pi} \int_0^\infty d\omega J(\omega) \frac{\exp(-i\omega t)}{1 - \exp(-\beta\hbar\omega)}, \quad (4)$$

where a Lorentzian spectral function has the form $J(\omega) = 2\lambda\omega/(\omega^2 + \gamma^2)$. For simplicity in this work we have considered a single Lorentzian term with amplitude $\lambda = 35\text{cm}^{-1}$ and cutoff frequency $\gamma = 50\text{cm}^{-1}$. However these values were actually extracted by fitting the experimentally measured absorption spectrum using an Ohmic spectral density $J(\omega) = \lambda(\omega/\gamma) \exp(-\omega/\gamma)$ [72]. Thus, we also examine ETE versus variations of λ and γ in such a model depicted in Fig. 18, see appendix B. We note that for an Ohmic model a very similar behavior of the optimality and robustness of energy transport can be observed as those in Fig. 2; however, the estimated ETE is lower than those obtained by exploiting a Lorentzian model. Specifically for FMO the ETE value are 92.3% and 96.7% for Ohmic and Lorentzian spectral density respectively. This suggests that an Ohmic bath can not capture the near unity efficiency of FMO complex, and favors the Lorentzian model as a more accurate description of the bath spectral density.

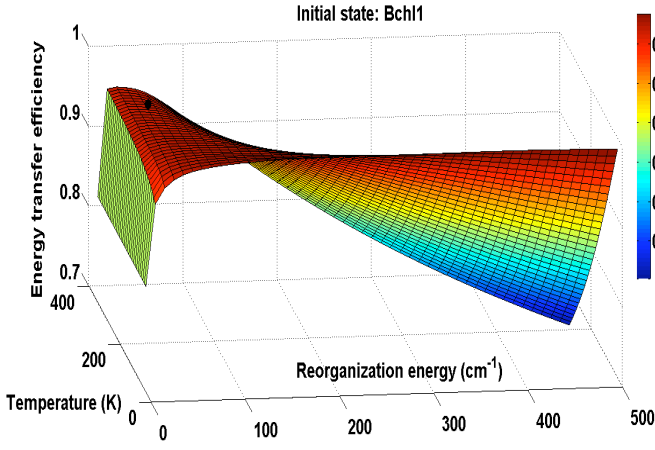


FIG. 5: Energy transfer efficiency manifold as a function of reorganization energy and temperature. The temperature range is from $35^\circ K$ to $350^\circ K$. At the regimes of large system-bath coupling strength the ETE drops faster by increasing the temperature due to strong localization induced by dynamical disorder. There is a narrow region of reorganization energies between 10 and 50 cm^{-1} that ETE is relatively robust with respect to variations in temperature. The FMO value of $\lambda = 35 \text{ cm}^{-1}$ is located in this region indicating a significant insensitivity to temperature variations. At very low reorganization energy and low temperatures weak localization can be observed due to static disorder.

B. Reorganization energy and Temperature

Here, we directly examine the temperature dependence of the effective parameter λ/γ discussed in the pervious section. Generally light-harvesting complexes in bacterial, marine algae, and higher plants operate at various temperatures and reorganization energies. For example, the FMO complex of the green sulfur bacteria can operate at the bottom of the ocean at a depth of hundreds of meters, and also in hot springs with diverse temperature variations. Moreover, 2D electronic spectroscopy of these systems have been performed at different cryogenic and room temperatures. Thus, we need to explore the efficiency and sensitivity of energy transport as a function of reorganization energy and temperature.

We note that in the low temperature limit, $\beta > \gamma^{-1}$, the Lorentzian bath correlation function $\langle \tilde{B}(t)\tilde{B}(t') \rangle_{ph}$ is no longer a single term $\lambda(2/\beta - i\gamma)e^{-\gamma(t-t')}$ and should be corrected by a sum of exponentially decaying terms

$$\langle \tilde{B}(t)\tilde{B}(t') \rangle_{ph} = \frac{\gamma\lambda}{\hbar} \left(\cot\left(\frac{\beta\hbar\gamma}{2}\right) - i \right) e^{-\gamma(t-t')} + \frac{4\lambda\gamma}{\beta\hbar^2} \sum_{k=1}^{\infty} \frac{\nu_k}{\nu_k^2 - \gamma^2} e^{-\nu_k(t-t')} \quad (5)$$

where $\nu_k = 2\pi k/\beta\hbar$ are bosonic Matsubara frequencies. In practice a truncation of the above infinite series is needed for numerical simulations. The higher levels of truncation are dictated by lower temperature limits for the systems under study. To guarantee an accurate estimation of the bath correlation

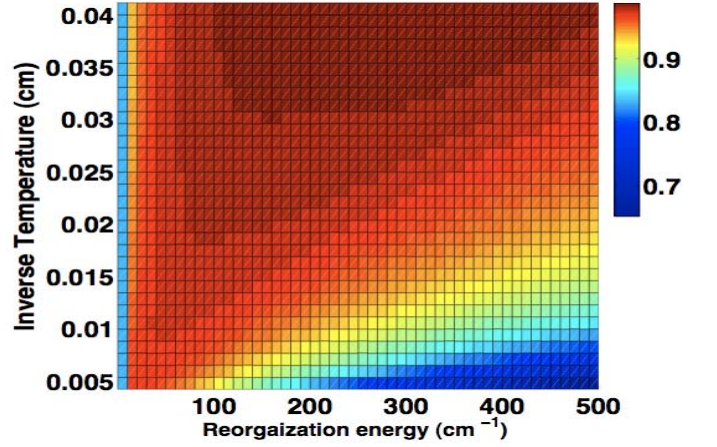


FIG. 6: The top view of the ETE landscape presented in Fig. 5 as a function of inverse temperature and reorganization energy. In the high temperature regime ($\beta^{-1} > \gamma$), the three regions of weak localization, ENAQT and strong localization can be distinguished by the parameter λT given the free Hamiltonian of FMO and $\gamma = 50 \text{ cm}^{-1}$. These results, combined with Fig. 3 suggest that the parameter $\lambda T/\gamma$ governs the shape of the overall FMO energy transfer landscape.

function for the calculation of energy transfer landscape, in the relevant low temperatures, we consider the first one hundred Matsubara frequencies in the above summation. It should be noted that the mentioned low temperature corrections have a minor numerical cost for calculating ETE by using TC2 (2), since we just need to compute sum of the Laplace transforms of the above exponential terms [55]. This is another advantage of using the TC2 in contrast to the more accurate approaches such as HEOM for which every correction term $\nu_k e^{-\nu_k(t-t')}$ necessitates considering N extra auxiliary variables in the simulation, where N is the number of the sites, therefore significantly increasing the computational cost of the simulations.

We show the behavior of ETE as a function of reorganization energy λ and temperature T in Fig. 5. It can be observed that at various possible conditions for the FMO protein of $T = 280$ to $350^\circ K$ and $\lambda = 35 \text{ cm}^{-1}$, the ETE has an optimal value and resides in a robust region of the energy transfer landscape. We note that for system-bath strength corresponding to the FMO's environment, the energy transport is very robust to variations of temperature and just slightly decreases in the low temperature limit. By increasing the reorganization energy, the temperature dependence of ETE becomes more pronounced. As we move toward the classical regime of the dynamics at high reorganization energy and high temperature ETE drops significantly. This implies the necessity of quantum effects for highly efficient and robust excitonic energy transfer. It is remarkable that at the relevant physiological temperatures, the ETE is robust only within the range of $\lambda = 35 \text{ cm}^{-1}$, and it becomes unstable as we approach reorganization energy of over 100 cm^{-1} . On the other hand, at the very low temperatures, enhancement of λ would improve the ETE and brings it to a saturated high level. The gradient

and Hessian norms as functions of reorganization energy and temperature are illustrated in Fig. 7. At the relevant FMO operating temperatures, optimum and robust energy transport can occur simultaneously only within a small regions of λ between 30 to 35 cm^{-1} , which coincide with the estimated values of reorganization energy for the FMO. We note that there are certain regions of higher robustness at higher reorganization energy that are in principle available, but these regions imply a significantly lower operating temperature for the FMO operation and they have suboptimal ETE in comparison with actual FMO environmental parameters at the room temperature.

As shown in the previous section, the parameter λ/γ governs the shape of the ETE landscape at a fixed high-temperature limit. However, in the perturbative limit the decoherence rate can be expressed by $\lambda T/\gamma$ which captures the suboptimal ETE in the weak localization region. Now, we investigate if the ETE behavior in all regimes can be globally captured by the parameter $\lambda T/\gamma$, for the given FMO Hamiltonian. Specifically, we need to verify if one can predict the optimal noise-assisted transport region as well as ETE suppression levels at the strong localization regions by a single parameter $\lambda T/\gamma$. To examine the validity of this theory, we study ETE as a function of the reorganization energy and the inverse temperature for the fixed $\gamma = 50 cm^{-1}$, see Fig. 6. Similar to the plot of efficiency as a function of λ , γ , Fig. 3, here also the efficiency landscape is divided by lines of approximately λT (with some deviations from linearity in the high λ and low temperature regime). It can be observed from the Fig. 6 that for small λT weak localization is dominant. At the intermediate λT values environment-assisted energy transport occurs. As we move towards larger system-bath interactions and higher temperatures, strong dynamical disorder diminishes the coherence and the exciton migration can be fully described by an incoherent hopping process, since the wave function is essentially localized over spatial sites. At this regime, the effect of high temperature can be understood from the dynamics of BChls energy fluctuations which is described by the symmetrized correlation function $S(t) = \frac{1}{2}\langle\{\hat{B}(t), \hat{B}(0)\}\rangle_{ph}$ ($B_j = B$, for any BChl j). The function can be extracted experimentally by three-pulse photon echo peak shift measurement. For a Lorentzian density, $S(t) = 2\hbar\lambda/\beta e^{-\gamma t}$, and fixed γ , the temperature and the reorganization energy determines the amplitude of the site energy fluctuations. Our simulation in Fig. 5 demonstrates that a high efficient energy transfer can be achieved at a *moderate* site energy fluctuations away from both weak and strong localization limits.

Combining different regimes of three important environmental parameters, λ , γ , and T , the effective decoherence strength $\lambda T/\gamma$ emerges as the parameter that governs the energy transfer efficiency landscape. For the FMO free Hamiltonian energy gaps, by increasing the single parameter $\lambda T/\gamma$ from small to intermediate, and from intermediate to large values, one can describe the transition from weak localization to ENAQT, and from ENAQT to strong localization. More generally, when the effective decoherence rate $\lambda T/\gamma$ is either much smaller or much larger than the typical energy splitting g

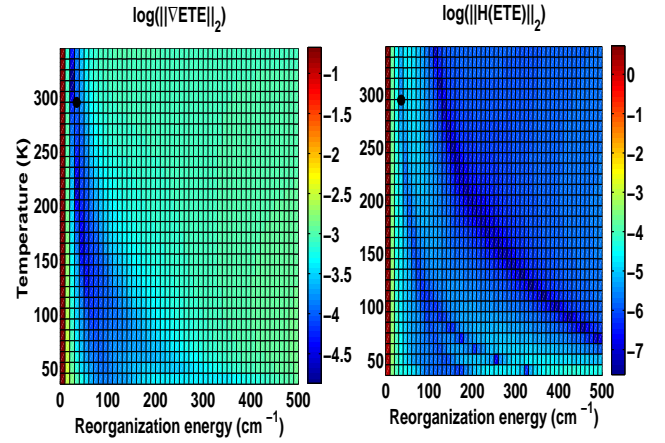


FIG. 7: This figure is a complement to Fig. 5. Left: the degree of ETE optimality is quantified at different values of λ and T by the norm of the ETE gradient. The dark blue points represent near optimal values. Right: the degree of ETE robustness is quantified by the Euclidian norm of the ETE Hessian. The dark blue points represent near robust points. We note that within the range of possible FMO operating temperatures (e.g between $T = 280^\circ K$ to $T = 350^\circ K$) simultaneous optimal and robust energy transport can only be achieved for λ values around 30 to 35 cm^{-1} , that is equivalent to the estimated reorganization energy for the FMO complex that is marked by a black dot at room temperature $T = 298^\circ K$.

between delocalized energy eigenstates, then transport is suppressed. Thus, in order to predict the general patterns of quantum transport in generic light-harvesting systems, we should compare the relative strength of $\lambda T/\gamma$ (with dimension of energy) to the average excitonic energy gap of the free Hamiltonian that can be quantified as $g = \frac{1}{N-1}\|H - Tr(H)\mathbb{I}/N\|_*$ for an N level system, where the nuclear norm $\|X\|_*$ is defined as the summation of X 's singular values. This follows from the fact that the ETE of a system with a rescaled Hamiltonian αH equals the ETE of a system with Hamiltonian H for which other environmental energy/time scales are renormalized by a factor $1/\alpha$. Here we give a simple proof for this fact:

The efficiency defined in Eq. (3) can be simply calculated as $\eta = 2r_{trap}\langle trap|\tilde{\rho}(s=0)|trap\rangle$ where \sim denotes the Laplace transform. The operator $\tilde{\rho}(s=0)$ can be found by transforming the dynamical equation (2):

$$\begin{aligned} -\rho(0) &= \mathcal{L}_S \tilde{\rho}(0) + \mathcal{L}_{e-h} \tilde{\rho}(0) \\ &- \sum_j [S_j, \frac{1}{\hbar^2} \tilde{C}(-\mathcal{L}_S) S_j \tilde{\rho}(0) - h.c.]. \end{aligned} \quad (6)$$

This yields the ETE

$$\eta = -2r_{trap}\langle trap|\mathcal{K}\rho(0)|trap\rangle \quad (7)$$

where

$$\mathcal{K} = (\mathcal{L}_S + \mathcal{L}_{e-h} - \sum_j [S_j, \frac{1}{\hbar^2} \tilde{C}(-\mathcal{L}_S) S_j - h.c.])^{-1} \quad (8)$$

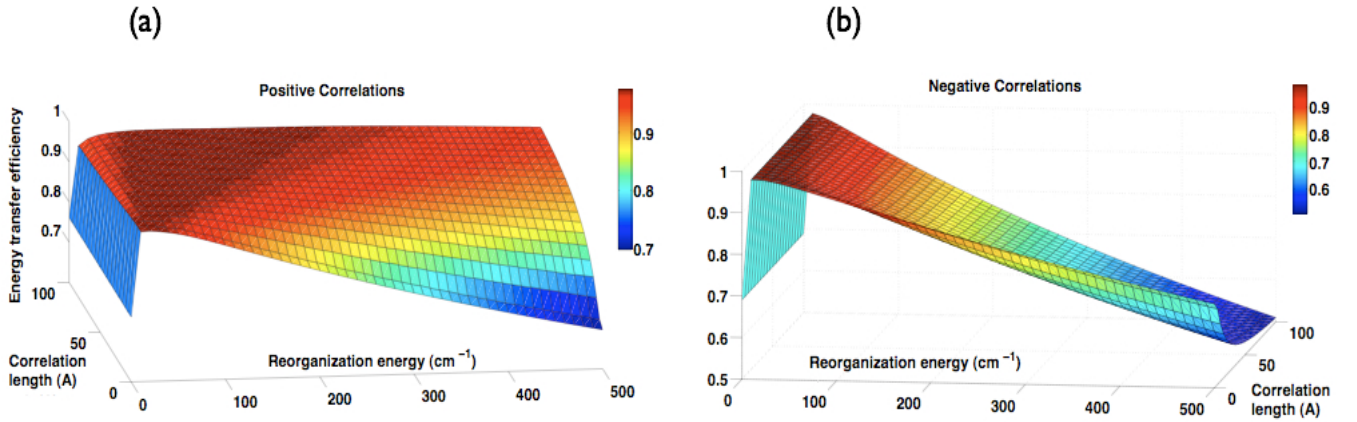


FIG. 8: (a) ETE as a function of reorganization energy and positive bath spatial correlations that correspond to in-phase fluctuations of two spatially separate bath oscillators. At the large values of reorganization energy, the positive correlations induce certain symmetries in the effective phonon-exciton Hamiltonian significantly enhancing ETE, by protecting the system against strong dynamical disorder similar to decoherence free subspaces [79]. In the intermediate values of λ , the ENAQT become more robust due to spatial correlations. In large correlation length, the optimal ETE is essentially expanded over a much wider regime, one order of magnitude larger than the optimal ETE region in the absence of any spatial correlations. At smaller values of λ positive spatial correlations actually hinder the exciton transport by decoupling useful but very weak fluctuations. A similar linear relationship is observed here between λ and positive spatial correlations as those with γ and T . (b) ETE as a function of reorganization energy and negative spatial correlations that correspond to out of phase fluctuations of two spatially separate bath oscillators. Negative correlations reduce ETE at all values of λ .

The Laplace transform of the correlation function (5) can be found as $\tilde{C}(-\mathcal{L}_S) = \frac{\gamma\lambda}{\hbar(\gamma-\mathcal{L}_S)}(\cot(\frac{\beta\hbar\gamma}{2}) - i) + \frac{4\lambda\gamma}{\beta\hbar^2} \sum_{k=1}^{\infty} \frac{\nu_k}{(\nu_k^2 - \gamma^2)(\nu_k - \mathcal{L}_S)}$. Considering these explicit expressions, it is easy to see that the system-bath parameters $\{\alpha H, \lambda, \gamma, T, r_{trap}, r_{loss}\}$ yields the same ETE (7) as the parameter set $\{H, \lambda/\alpha, \gamma/\alpha, T/\alpha, r_{trap}/\alpha, r_{loss}/\alpha\}$. We should mention that similar results can be obtained for the hierarchy equation of motion.

Overall, we introduce the dimensionless parameter as $\Lambda = \lambda T/\gamma g$, as the parameter that governs the energy transfer efficiency landscape. When we approach $\Lambda \approx 1$, the decoherence rate is tuned to give the maximum transport rate. For $\Lambda \ll 1$ and $\Lambda \gg 1$ we move toward weak and strong-type of transient localizations respectively. To examine the temperature and also spectral density independency of the observed patterns in Figs. 3 and 6, we present the landscape top view of ETE for a) Lorentzian density at $77^\circ K$ and b) Ohmic density at $298^\circ K$, in appendix B. In both cases a similar pattern can be observed.

In the subsequent sections, we fully explore the interplay of reorganization energy with a variety of Frenkel-exciton free Hamiltonians for systems consist of up to 20 chromophores with modest site energetic disorders. Our numerical studies suggest that in the optimal transport regime the relevant energy scale of the free Hamiltonian, g , can be essentially expressed as the average dipole-dipole interactions strength that is $|\mu|^2 n$, where is $|\mu|^2$ is the average dipole-moment strength and $n = \frac{8N}{D^3}$ is the density of N chromophores homogenously embedded in a system with size D . We will address the significance of the convergence of energy scales in the broader context of complex quantum systems in the discussion sec-

tion.

C. Reorganization energy and bath spatial correlations

Recently there have been significant interest on the potential role of bath spatial correlations as the underlying physical principle leading to the experimental observations of long-lived quantum coherence in biomolecular systems [20, 21, 26]. These correlations have also been the center of attention and debate in the recent theoretical studies of quantum effects in photosynthetic complexes [30, 74–76] as a potential positive feature of environmental interactions. The basic intuition is that if the environmental fluctuations are correlated in space, e.g., in the site basis, then they will lead to fairly global quantum phase modulations in exciton basis, similar in spirit to *decoherence-free subspaces* that are studied in details in quantum information science [79]. Indeed, as demonstrated earlier in Ref. [30], using a Lindblad master equation, positive spatial correlation can enhance the underlying contributions of quantum coherence to ETE according to two different measures based on Green's function methods. However, the overall ETE remains relatively unchanged for the FMO estimated values, as the contribution of relaxation to ETE drops with a similar rate Ref. [30]. Here, we are interested in the potential role of quantum correlations in optimality and/or flexibility of energy transport rather than enhancing the time-scale of quantum coherence beating.

The TC2 can be generalized to include the effect of both spatial and temporal correlations between protein environ-

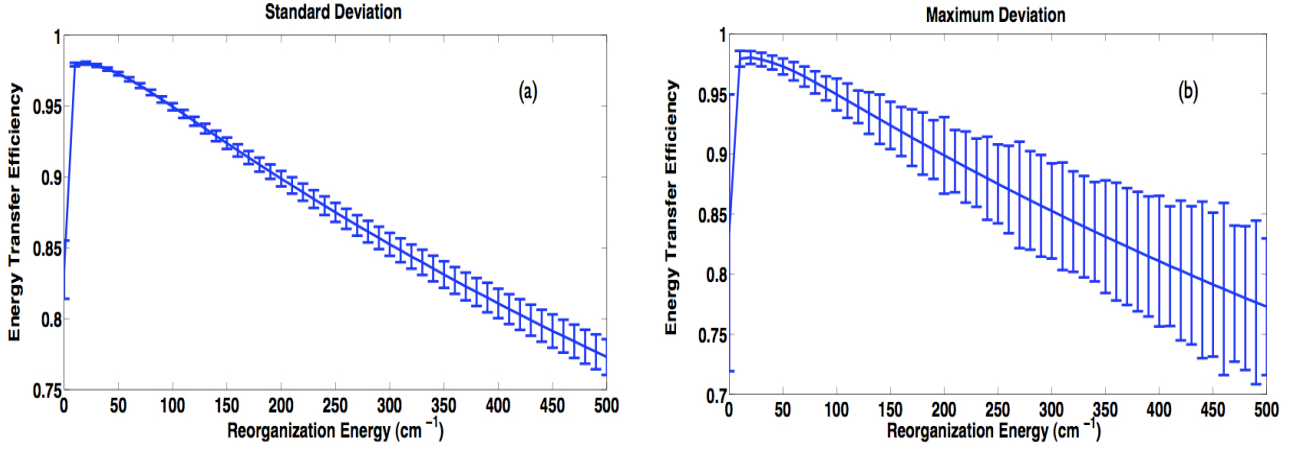


FIG. 9: The degree of sensitivity of ETE for 10^4 uniformly sampled pure and mixed initial exciton density matrices for different values of reorganization energy: (a) The error bars indicate the ETE standard deviation. At the FMO value of $\lambda = 35\text{cm}^{-1}$ the standard deviation of ETE has a negligible value of about 0.1%. (b) A worst-case scenario of FMO energy transport sensitivity to initial exciton states. Here, the error bars indicate the maximum and minimum values of ETE achieved over the sample of 10^4 randomly chosen initial states. At the FMO value of $\lambda = 35\text{cm}^{-1}$ the variation in ETE is less than 1%

ments:

$$\begin{aligned} \frac{\partial}{\partial t}\rho(t) &= \mathcal{L}_S\rho(t) + \mathcal{L}_{e-h}\rho(t) \\ &- \sum_{j,k} [S^j, \frac{1}{\hbar^2} \int_0^t C_{j,k}(t-t')e^{\mathcal{L}_S(t-t')} S^k \rho(t') dt' - h.c.] \end{aligned} \quad (9)$$

The function $C_{j,j}$ is just the autocorrelation function of the j th environment. The cross correlation between fluctuations of sites j and k is given by the function $C_{j,k}(t-t') = \langle \tilde{B}_j(t)\tilde{B}_k(t') \rangle$. In our study we assume $C_{j,k}$ to be of Lorentzian $\lambda_{j,k}\gamma\omega/(\gamma^2 + \omega^2)$ form with the cut-off frequency γ , similar to the autocorrelation spectral density, and the strength $\lambda_{j,k}$ that decays exponentially with the distance between Bchls j and k , $d_{j,k}$. A correlation length R_{cor} determines the strength of the spatial correlations, $\lambda_{j,k} = \lambda \exp(-d_{j,k}/R_{cor})$. We distinguish between the two different cases of positive and negative correlations, corresponding to $\lambda > 0$ and $\lambda < 0$ respectively. The sign of the correlations is imposed by the position and orientation of the Bchls with respect to their surrounding protein [77].

The effects of positive and negative spatial correlations on the energy transfer efficiency for various degrees of the system-bath couplings are presented in Fig. 8. One main observation is that both positive or negative spatial correlated environmental fluctuations play an insignificant role in the overall ETE only at the regions of reorganization energy very close to $\lambda = 35\text{cm}^{-1}$. However, as we slightly increase the system-bath coupling strength, we see two very distinct behaviors of the ETE as a function of long-range spatial characteristics of the bath fluctuations, depending on whether these variations being correlated or anti-correlated. For rather strong reorganization energy, positive spatial correlations can enhance the ETE by about 30%. By contrast, negative spatial correlation can reduce the ETE by the same amount for reorganization energy of above $\lambda = 400\text{cm}^{-1}$.

A careful inspection of Fig. 8 (a) shows a linear relationship between reorganization energy and positive spatial correlations similar to those with γ and T , as discussed in the previous section. For very small reorganization energies, when quantum localization due to static disorders is present, the positive spatial correlations can slightly reduce ETE by decoupling the fragile but positive role of environmental fluctuations. On the other extreme regime, positive spatial correlations can play a significant positive role by inducing an effective *symmetry* in the system-bath interactions, leading to partial immunity with respect to the strong dynamical disorders at large reorganization energies. Remarkably, in the intermediate regime, the induced symmetries can substantially enhance the robustness of the environment-assisted transport. We can observe that the width of ENAQT region (in reorganization energy axes) is enhanced from 20cm^{-1} for zero correlation length to 200cm^{-1} for 100\AA correlation length. At this wide regimes, the system is protected with respect to the adversarial effects of dynamical disorder preventing the strong localization effects. Therefore, the spatial correlations should be also incorporated in the governing parameter $\lambda T/\gamma$. This can be achieved by renormalizing the reorganization energy λ to an effective lower/higher values, when positive/negative correlations exist.

In order to quantify the role of spatial correlations in enhancing the quantum coherence time-scale of light-harvesting complexes, one has to partition the time-nonlocal master equation, Eq. 2, similar in spirit to those studies in Ref. [30, 38]. In the other sections of this work we assume spatial correlations to be negligible for the FMO complex consistent with the recent simulations in Ref. [78]. Indeed, the atomistic simulation of the FMO pigment-protein-solvent dynamics at room temperature presented in Ref [78] reveals insignificant correlations in the site energy fluctuations, suggesting that the uncorrelated bath approximations are reasonably valid. Next, we explore the role of initial conditions.

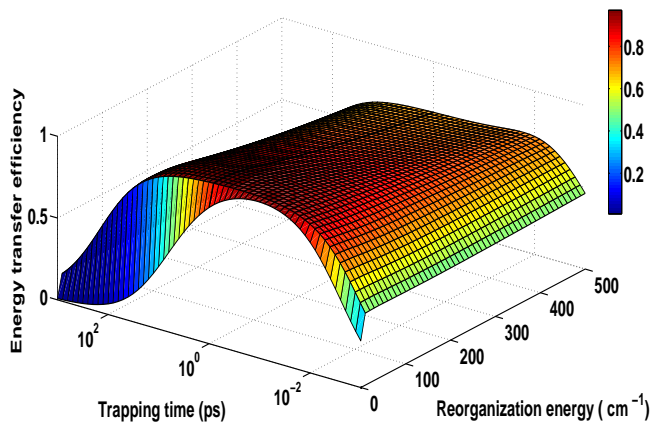


FIG. 10: The ETE manifold on the parameter space of reorganization energy and trapping time-scale. It can be seen that the FMO complex reaches its maximum functionality at trapping rates of about $0.5 - 5 \text{ ps}^{-1}$. The tunnel-shape ETE landscape can be understood by noting that at low trapping rates the transport efficiency is diminished by the recombination process. At high trapping rates the exciton transfer is suppressed via quantum Zeno effect as the trapping process corresponds to very strong and continuous measurement of the system.

IV. ENERGY TRANSPORT SENSITIVITY ON THE INITIAL EXCITATIONS

The exciton migration pathways and time-scales have been studied in detail for a variety of light-harvesting complexes using various perturbative techniques including Förster models for studying LHI and II of purple bacteria [9] and Lindblad models for simulating the dynamics of the FMO protein of green sulphur bacteria [29]. Nevertheless, the role of initial conditions in the overall energy transfer efficiency of photosynthetic complexes is to a large extent unknown. It was recently shown that the initial quantum coherence could influence the energy transfer efficiency in LHI of purple bacteria assuming no interaction with the phonon bath [34]. The dependency on initial localized excitation at BChls 1 and 6 were also examined for the FMO complex using Lindblad, Haken-Strobl, and HEOM models [29, 31, 37]. However, the sensitivity of ETE with respect to generic initial pure and mixed states taken from a large ensemble in the single-excitation manifold has not previously been explored.

Here, we first examine the average sensitivity of ETE with respect to randomly chosen initial states for various reorganization energies. To this end, for each value of reorganization energy, we sample over 10^4 (pure or mixed) density matrices from a uniform distribution in the space of all 7×7 trace one positive matrices. In Fig. 9 (a) the average values of ETE is plotted with an error bar representing the variance of ETE in our random sampling. Note that at the optimal ETEs, corresponding to the value of reorganization energy of the FMO complex, the dependency of the variances on initial states is very small – less than 0.1%. However, the ETE fluctuations can grow by an order of magnitude for larger or smaller values of λ . We also investigate the best and worst possible random

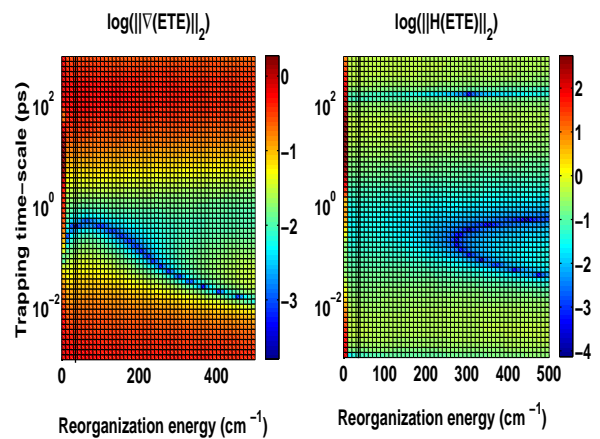


FIG. 11: This figure is a complement to Fig. 10 (Left). The degree of ETE optimality is quantified at different values of λ and r_{trap}^{-1} by the norm of the ETE gradient. The dark blue points represent near optimal values. (Right) The degree of ETE robustness is quantified by the Euclidian norm of the ETE Hessian. The blue points represent near robust points. The FMO achieves its maximum efficiency at $r_{trap}^{-1} = 0.5 \text{ ps}$. Note that for larger reorganization energies the trapping rate has been increased to achieve optimal ETE. However, this competition does not exist at small and intermediate system-bath coupling strength, where λ is on the order of off-diagonal elements of the FMO free Hamiltonian leading to environment-assisted energy transport. This suggests that a general convergence of time-scale might be required to obtain global efficient and robust transport (see discussion section). Although certain regions of highly robust ETE can be observed in figure (b), but those cases are suboptimal by considering their corresponding values in figure (a).

initial single excitonic states in the Hilbert space of FMO. In Fig. 9 (b), we illustrate this extreme possible deviations by error bars on the average ETE at any given value of λ . Note that ETE is very robust, varying about 1% with respect to different initial excitations at the optimal area of ETE landscape. However, this robustness diminishes substantially at the regimes of large reorganization energy. Next, we study the ETE landscape as a function of trapping and dissipation rates.

V. TEMPORAL AND GEOMETRICAL EFFECTS OF THE TRAPPING MECHANISM

Basic structural information on the FMO-RC complex has been obtained via linear dichroism spectra and electron microscopy [80]. These studies indicate that the symmetry axis of the trimer is normal to the membrane containing the reaction center. The electron microscopy resolution is generally not sufficient to distinguish the top and the bottom of the FMO trimer nor the distance between FMO-RC. Thus, in principle either pairs of BChls 1 and 6 or BChls 3 and 4 are the pigments that connect the FMO complex to RC. However, it is widely believed, due to efficient energy funneling toward RC, that BChl 1 and 6 are the linkers to antenna baseplate, and 3 and 4 should serve as target regions within the neighbourhood of RC complex [16]. This hypothesis has been recently veri-

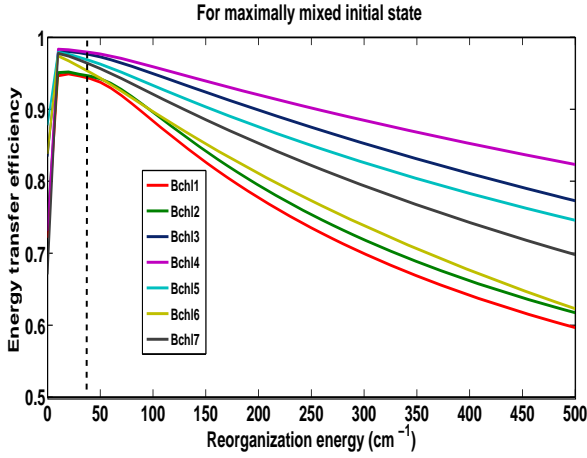


FIG. 12: The ETE as a function of reorganization energy for the initially maximally mixed state. In each plot one of the 7 BChls is considered to be connected to the reaction center. BChls 3 and 4 acting as the exciton transfer bridge yield the highest efficiency for almost all values of the reorganization energy. This confirms the experimental evidence that the FMO spatial orientation is such that the BChls 3 and 4 are located near the RC.

fied experimentally [81]. Up to this point, we have considered BChl 3 to be in the close proximity of RC by a trapping time-scale of about $1 ps$. However, in this section we consider both of these parameters to be free, in order to explore the optimality and robustness of the ETE landscape as we vary the time-scale and geometrical constraints set by the RC trapping mechanism.

In Fig. 10, we study the behavior of energy transfer efficiency landscape in various trapping time-scales and reorganization energies. It is evident that as the trapping rate becomes very slow comparable to $100 ps$ or slower, the ETE drops significantly independent of the values of λ . This can be understood intuitively as follows: the excitation has to wait on average so long for successful trapping to take place such that there will be an increasing chance of electron-hole recombination as we are approaching time-scales comparable to exciton life time. If the trapping mechanism occurs within a time-scale of $1 ps$, the ETE reaches to its expected maximum value of about 99%. Generally, one might expect that with increasingly faster trapping mechanisms the likelihood of dissipation to environment vanishes and energy transport approaches to the ideal case of having perfect efficiency. However, when the trapping rate becomes very fast on the order of $10^{-2} ps$ or faster, the ETE also drops significantly, a result that might appear counter-intuitive. In fact, overly rapid trapping leads to low efficiency via the quantum Zeno effect, as the rapid trapping effectively freezes the exciton dynamics and prevents it from entering the reaction center. As a result, the finite exciton life-time eventually leads to complete dissipation of excitation to the environment in extreme limit of fast trapping of about $1 fs$.

The optimality and robustness of ETE versus both decoherence and trapping rates using gradient and Hessian norms are presented in Fig. 11 (left panel). It can be observed that at

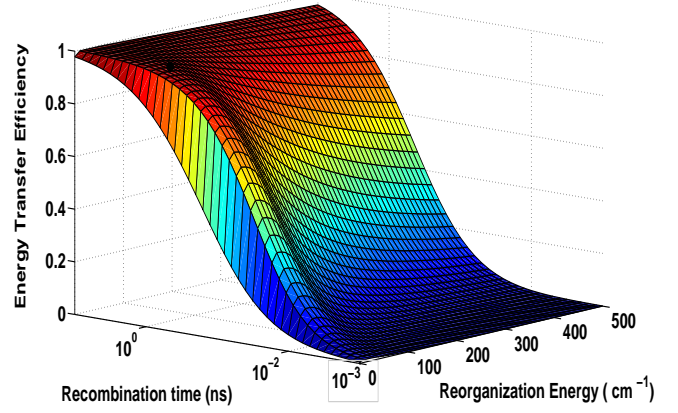


FIG. 13: ETE versus dissipation (loss) time-scale r_{loss}^{-1} and reorganization energy. The maximum optimality and robustness for FMO is observed around the estimated value $r_{loss}^{-1} = 1 ns$ implying the significance of the time-scale separation between dissipation and trapping rates. We note that the ENAQT effect is ubiquitous at all rates of electron-hole recombination process.

$\lambda = 35 cm^{-1}$ for the FMO, the ETE is optimal with a trapping rate of about $0.5 ps$. If the environmental interactions were stronger, a comparably faster trapping mechanism would be required to preserve such high level of efficiency. However, for small and intermediate system-bath interaction strength, where environment-assisted transport occurs, slower trapping rates become optimal, that is λ and r_{trap} are not competing processes anymore. This implies that a multi-parameter convergence of time-scales of the relevant physical processes might be required for light-harvesting complexes to operate optimally. We will address this issue in a broader context in the discussion section. From Fig. 10, it can be easily seen that ETE is very robust to variation of trapping rate at about $1 ps$ time scale. In Fig. 11, we also illustrate the robustness with respect to both trapping and reorganization energy (right panel). For rather large values of λ , there are certain regions that are highly robust to both parameters, but they are in fact suboptimal, as can be seen from noting their values in the left panel.

To explore the optimality of ETE with respect to the location of reaction center, we consider the efficiency of other scenarios that the reaction center can be in the proximity of any other BChl sites. Figure 12 shows a cross-section of Fig. 2, in a fixed $\gamma = 50 cm^{-1}$, for all possible trapping sites. To be unbiased with the respect to the initial state, we assume a maximally mixed initial state. It can be seen that the optimal curves belong to BChls 3 and 4 as expected, since they contribute highly to the lowest energy delocalized excitonic states. It should be noted that optimal environment-assisted quantum transport, and the two extreme regimes of quantum localization can be observed for all of these plots independent of the actual location of trapping. In other words, the behavior of the energy transport efficiency landscape and its dependence on a single governing parameter are not properties of a particular choice of trapping site in the FMO structure.

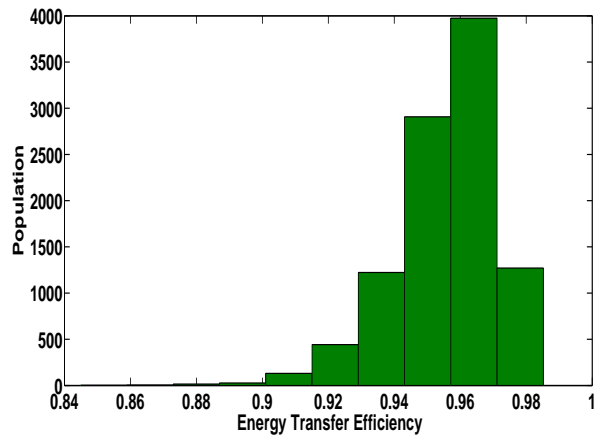


FIG. 14: Robustness of FMO transport efficiency with respect to small variations of BCHls locations, site energies and dipole orientations for 10000 samples: the Hamiltonian parameters are perturbed with site energies disorders of $\pm 10 \text{cm}^{-1}$, dipole-moment uncertainties of $\pm 5^\circ$, and BCHls spatial displacement of $\pm 2.5 \text{\AA}$. The statistical distribution of 10^4 random configurations shows a significant degree of robustness such that 99% of samples still preserve an efficiency of above 0.9.

For completeness, we also investigate the ETE landscape as a function of dissipation (loss) rate and reorganization energy in Fig. 13. In our simulation of the FMO dynamics we have used the estimated value of $r_{\text{loss}}^{-1} = 1 \text{ns}$. In Fig. 13, however, we treat loss rate as a free parameter and we observe that for any stronger dissipation process, ETE would have a suboptimal and less stable behavior. Thus, even if all the other important parameters are within the optimal regime, a large time-scale separation between dissipation and trapping rate is still required to guarantee the highest performance for light-harvesting complexes. Fig. 13 also demonstrates that the existence of ENAQT is independent of a particular choice of dissipation rate.

VI. OPTIMALITY AND ROBUSTNESS WITH RESPECT TO PARAMETERS OF FMO HAMILTONIAN

So far, we have demonstrated that for the estimated Hamiltonian elements of the FMO complex, the environmental parameters and trapping rates are within the right set of values leading to an optimal noise-assisted energy transfer efficiency. Moreover, the performance of FMO is robust with respect to variations in such decohering and lossy processes and to uncertainties in initial conditions. However, in the context of exploring the role of coherent system evolution, it is not fully clear if the FMO internal Hamiltonian parameters have evolved to function optimally and fault tolerantly, despite disorders and thermal fluctuations. This issue has been examined for LHCI in Ref. [82] using semi-classical Pauli master equations to simulate the exciton dynamics. Here, we would like to use TC2 to explore how rare is the FMO geometry in terms of its efficiency, whether the specific spatial and

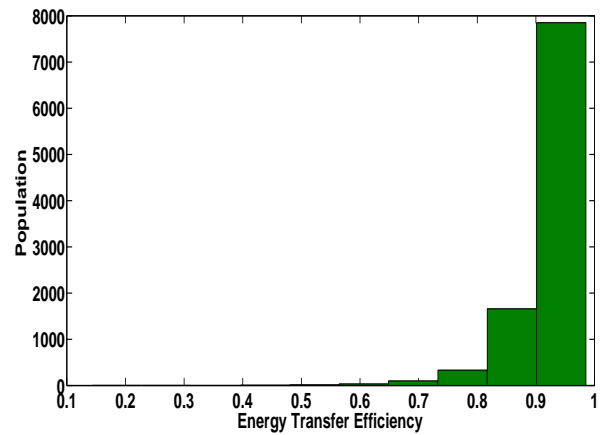


FIG. 15: Robustness of the FMO complex transport efficiency with respect to large variations in BCHls site energies and dipole moment orientations for 10000 sample configurations: While the location of BCHls are still slightly perturbed, similar to Fig. 14 of about $\pm 2.5 \text{\AA}$, the dipole moments can take any arbitrary direction and site energy takes any value between zero and 500cm^{-1} . This Histogram reveals that the relative distance of BCHls is playing a crucial role in performance of these random light-harvesting complexes since 79% of them still hold ETE larger than 90%.

dipole moment arrangements of BCHls are essential for such highly efficient functioning of this pigment-protein complex, and how robust these parameters are with respect to small and large perturbations in chromophoric distances, dipole moment orientations, and site energy fluctuations. Specifically, we explore if the FMO closely packed structure plays any functional role, and illustrate a potentially important convergence of the relevant dynamical time-scales in the FMO energy transport. In the following section, we investigate the underlying physical principle of quantum transport in more generic multichromophoric structures beyond the FMO geometry. We examine the efficiency of small light-harvesting complexes as functions of the compactness level, number of sites, reorganization energy, exciton energy gaps, and multichromophoric connectivity.

The Frenkel exciton Hamiltonian for a multichromophoric system is expressed as:

$$H_S = \sum_{j,k} \epsilon_j |j\rangle \langle j| + J_{j,k} |j\rangle \langle k|, \quad (10)$$

in which J_{jk} are Coulomb couplings of the transition densities of the chromophores,

$$J_{jk} \sim \frac{1}{R_{jk}^3} (\mu_j \cdot \mu_k - \frac{3}{R_{jk}^2} (\mu_j \cdot \mathbf{R}_{jk})(\mu_k \cdot \mathbf{R}_{jk})), \quad (11)$$

where \mathbf{R}_{jk} denotes the distance between site j and k , and μ_j is the transition dipole moment of chromophore j [8]. We first study the robustness of free Hamiltonian parameters within the proximity of the estimated values for FMO as given in the appendix A.

A. Robustness of FMO Hamiltonian

Figures 14 and 15 demonstrate the robustness of the FMO structure to variations in its internal parameters. Figure 14 illustrates that FMO efficiency does not drop drastically with respect to variations in the dipoles orientations, site energies, and Bchls distances close to the neighborhood of the estimated values. Specifically, from 10000 random samples of FMO with spatial uncertainty around each Bchl location of about $\pm 2.5 \text{ \AA}$, dipole moments orientations variations of $\pm 5^\circ$, and site energy static disorder $\pm 10 \text{ cm}^{-1}$, 97% of configurations have efficiency of 95% or higher. This demonstrates a significant degree of robustness with small perturbations. In order to separate the influence of spatial coordinates from angular dipole orientations and disorders, we allow the latter two parameters to take arbitrary values from a large range while keeping Bchl locations uncertainties to be limited by $\pm 2.5 \text{ \AA}$. We observe in Fig. 15 that ETE remains relatively robust with 79% of random 10000 configurations have still efficiency of 90% or higher. This is rather counterintuitive considering huge freedom that we have accommodated in the dipole moment arrangements and site energies. These results indicate that spatial degrees of freedom is a dominating geometrical ingredient of the FMO structure and might play a key physical role in its performance.

B. Searching for FMO-type Hamiltonians

To explore the role of the free Hamiltonian parameters, we first investigated energy transfer efficiencies of 200,000 random 7-site chromophoric configurations embedded within a sphere of diameter 200 \AA , with random initial and target sites, and with environmental parameters the same as the estimated values of FMO [64]. We bounded the nearest distance among chromophores to be larger than 5 \AA , since the dipole-dipole approximation breaks down below this limit [18]. The dipole moment of each chromophore can take any orientation and the site energy of each chromophore can take any value between zero and 500 cm^{-1} chosen from a random distribution. We observed that only 10% of these configurations have efficiency larger than 50% and only 0.1% have efficiency comparable to FMO. Thus, one might conclude that the FMO structure is one of the rare geometries that can support this extremely high efficiency. However, as we argue below this conclusion is inaccurate.

We searched over various geometrical pattern correlations among the top 0.1% high-end efficient random structures to reveal the underlying principle(s) that could give rise to their high efficiency. We found that the distance between initial and target sites in most of these structures vary between $6 - 10 \text{ \AA}$. Thus most of these complexes are rather trivial optimal solutions that are not particularly interesting for quantum transport studies. Indeed each of those conformations essentially acts as a dimer including a donor and an acceptor chromophore that are strongly coupled via dipole-dipole interaction in the near field. This approach for optimality is obviously not usable for quantum transport in large natural or engineered light-

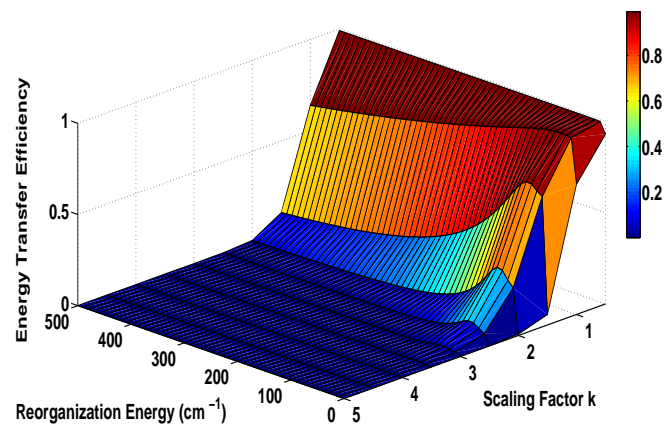


FIG. 16: Dependency of ETE on compactness level of the FMO complex. The FMO chromophoric spatial structure is scaled with a factor between 0.5 and 5. The ETE manifold is plotted as a function of the scaling factor and reorganization energy. For all levels of compactness, $\lambda = 30 - 40 \text{ cm}^{-1}$ yields the highest ETE. A more compact complex shows a higher degree of robustness with the respect to variation in reorganization energy. The scaling factor 1 corresponds to the FMO complex leading to a nearly optimal energy transfer efficiency.

harvesting antenna or macromolecular systems with typically significant spatial separation of initial excitation and trapping sites. In order to distinguish potential non-trivial optimal solutions hidden in these results; i.e., those involve quantum/classical jumps in a multi-path molecular networks, we consider the distance of donor and acceptor to be bounded by the size of the complex for the rest of our studies in this paper.

Our results presented in Figs. 14 and 15 clearly indicate that the relative Bchl locations play a major role in the overall performance of the FMO complex. Thus a potentially significant parameter of relevance is the compactness of a given pigment-protein complex. We further explore this feature by introducing a single *compactness* parameter by rescaling the Bchl distances by a factor k . We plot ETE as a function of compactness level k varying by an order of magnitude from 0.5 to 5. To explore any potential interplay of environmental interactions with this particular internal degree of freedom, we also simulate this size dependent supersession/enhancement of ETE in various reorganization energy, λ , in Fig. 16. It can be seen that transport efficiency drops significantly by expanding the FMO structure and has slightly enhanced value for contraction ratio of 0.5. As above, in the discussion of the evolutionary tuning of reorganization energies and environmental correlation times, it appears that nature has taken a rather minimal approach in designing FMO. By utilizing the right density level of chromophoric structure and strength of environmental interactions, the evolutionary process has created a nearly optimal energy transfer channel, but that process apparently avoided the extra work necessary for further compression to achieve just 1% or less enhancement in ETE. By inspection of the ETE variation with respect to λ in Fig. 16, one observes that the ENAQT phenomenon is scale invariant

for the FMO-like structure.

The above analysis reveals an important effective physical parameter; however, one cannot rule out the possibility of other underlying dynamical processes and/or geometrical correlations that could also lead to higher ETE in very different compactness regimes. In other words, the compactness appears to be a sufficient condition for high ETE in multi-chromophoric complexes but most likely it is not a necessary condition.

C. Convergence of time-scales for FMO

We illustrate a summary of our main results on the FMO complex energy transport dynamics in the non-Markovian and non-perturbative regimes in Fig. 17. This figure indicates that an effective convergence of time-scales for various dynamical processes exists at the intermediate and optimal regimes (denoted by a white circle) in the energy transfer landscape represented by a circular surface. The radius of this circular area illustrates the reorganization energy in logarithmic scale in the unit of time from $33.3ps$ (1 cm^{-1}) to $66.7fs$ (500 cm^{-1}). The circular area consists of four different regions in four quarters, the angular degrees of freedom in each quarter is associated to a different physical quantity. The first quarter represents the degree of the memory in the bath or the non-Markovity of the environment in logarithmic scale, that is equivalent to bath correlation time, varying from about $6.67ps$ to $66.7fs$. The second quarter illustrates variations in the bath temperature from 35 to 350 K . The third region shows six order of magnitude trapping time-scales from $1ns$ to $1ps$ in a logarithmic scale. The last quarter demonstrates compactness level of the Frenkel exciton Hamiltonian of the FMO rescaled by a factor from 0.5 to 5 . The estimated parameter of the FMO is denoted by a white bar in each region. In all quarters the efficient neighborhood of ETE are somewhere in the medium range, denoted by a white circle at about $1ps$ time-scale corresponds to reorganization energy of the FMO. The optimal areas are far from extreme low and high reorganization energies in the center and perimeter of the black circle respectively where quantum localization effects can substantially suppress ETE. The key point of this figure is that all the relevant useful transport time-scales converge just around $1ps$, far from the dissipation time-scale of $1ns$. We will discuss the implications of these results in a broader context of optimality and robustness of complex quantum systems in the next section.

VII. DISCUSSIONS ON THE CONVERGENCE OF TIMESCALES: QUANTUM GOLDBLOCKS PRINCIPLE

Our numerically study indicates optimality and robustness of FMO with respect to a variety of parameters. For FMO, in all cases, we find that the estimated operating values sit nearly at the optimal point for energy transport efficiency, and that there is a relatively wide range of parameters about that point for which FMO is close to optimal. Moreover, we note that the estimated time/energy scales associated with this

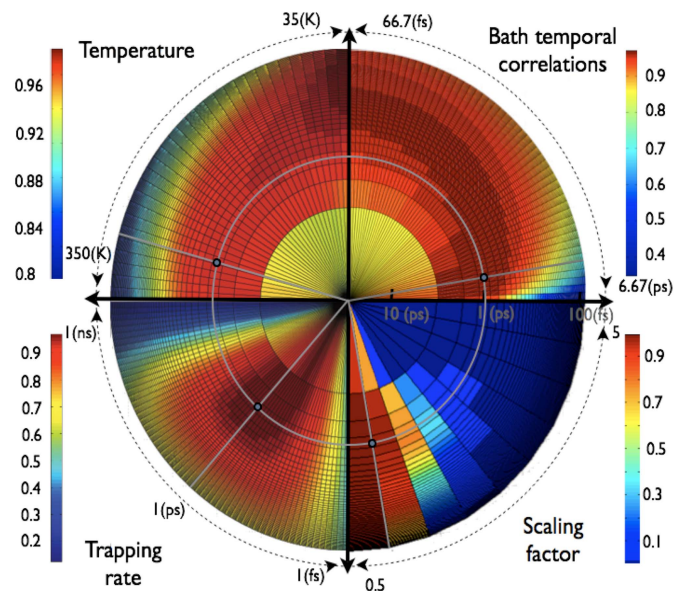


FIG. 17: A summary of our main results on the optimality and robustness of FMO energy transfer dynamics illustrating a convergence of time scale around $1ps$. The radial axes indicate the reorganization energy in logarithmic scale which is essentially the main environmental parameter quantifying the strength of system-bath interactions. Angular coordinate in each quarter represents a different physical quantity. The first three quarters are associated to three other important environmental parameters including bath correlation time-scale, temperature, and trapping time-scale. The last region highlights the role of compactness as the most significant internal parameter of FMO structure quantified by a rescaling factor in the chromophoric relative distances. To improve the clarity the color bar is rescaled in each quarter. The estimated values of the FMO complex coincide in the intermediate values of both angular and radial coordinates, denoted by white lines (around $1ps$), leading to optimal and robust ETE.

point – couplings between sites, reorganization energies, decoherence times, environmental correlation time, and trapping time-scale– all lie in the same intermediate range, on the order of a picosecond. Nevertheless it is instrumental for the FMO performance that life-time of exciton has a sufficiently longer time-scale. For alternative configurations, beyond the specific FMO model, we observe that their chromophoric density, geometrical arrangements, and coupling strengths need to be in tune with environmental interactions to lead to optimal performance. Here, we briefly discuss a design principle that fundamentally relies on this convergence of time scales.

A common design technique in engineering is to keep the desired system as simple as possible. The rationale is that overly complex designs are typically not robust: the more complex the design, the harder it is to predict its behavior, and the more pieces there are to fail. Now, FMO and other photosynthetic complexes are definitely not simple: they consist of multiple parts, and, as our studies show, enlist a wide variety of quantum effects, tuning those effects to attain efficient and robust operation. Apparently, these complexes do not obey the fundamental engineering philosophy of *keep it simple*. There is, however, a more sophisticated version of

the design principle in system engineering, as overly simple designs may be robust, but they typically also fail to attain their desired functionality. This advanced version of the design principle declares that to the extent that it is possible to add more features to a design to enhance functionality without reducing robustness, it is desirable to do so. That is, given available technologies, there is typically a design that attains a level of complexity that is ‘just right’ – not so simple that it fails to attain its goal, but not so complex that it loses robustnesses. The design strategy that aims for the just-right level of complexity is sometimes called the *Goldilocks principle* for complex systems [83]. Let’s look at how this principle applies in the case of the structure of FMO, a complex quantum system that has been evolved by natural selection.

The Goldilocks principle for complex quantum systems – the *quantum Goldilocks principle*– states that to improve efficiency, quantum effects could be used, as long as by doing so it does not make the operation of the system more fragile. Our simulations show that this is the case with FMO: a wide variety of parameters have been tuned to their optimal value, and that optimal value is robust against variations in those parameters. The quantum Goldilocks principle essentially explains why it is beneficial for certain parameters that involve time or energy to converge to the same time/energy scale.

When the time scale for one effect is very different from the time scale for another, then the first effect can typically be regarded as a perturbation on the other. For example, if the environmental interactions are much slower than the system internal dynamics, and/or if the correlation time of the environment is much shorter than the coherent tunneling rate of an exciton from chromophore to chromophore, then the effect of the environment can be treated in the perturbative and/or Markovian limits. If one effect is to interact strongly with another effect, by contrast, then the time/energy scales of the two effects should be similar. As we have shown here, the maximum efficiency of quantum transport is attained when the key decoherence parameter $\lambda T/\gamma$ is on the same order as the free Hamiltonian coherent time-scale g . As shown elsewhere [29, 31, 33, 67] environmentally assisted quantum transport is an important effect. This *convergence* of time scales is a nuisance for quantum simulation, as perturbative methods break down. While this phenomenon makes the efficient simulation of such systems very difficult, the convergence of time scales is quite useful for nature, however, as the two effects can now interact strongly with each other to produce a significant enhancement in efficiency. Of course, too strong interaction could also produce a significant decrease in efficiency. But for systems undergoing natural selection, one typically expect that the strong interaction is tuned at the right level to give rise to a beneficial effect.

The results of this manuscript illustrates the quantum Goldilocks principle manifestation in the FMO complex and other small-size multichromophoric configurations: the time/energy scales have converged within the range where the different quantum effects and structural parameters at work

can interact strongly with each other to give rise to possibility of high efficient energy transport. Moreover, this variety of quantum effects can be combined to attain high efficiency without sacrificing robustness. The convergence of time scales makes these complexes difficult to model, but highly efficient in certain instances. We anticipate that a similar convergence of time/energy scales could appear in larger biomolecular complexes and in biological processes where quantum mechanics might play an important role.

VIII. CONCLUSION

In this work, we studied the structural and dynamical design principles of excitonic energy transfer in the Fenna-Matthews-Olson (FMO) complex. Our numerical simulations demonstrate that the natural structure of FMO pigment-protein complex lead to a highly efficient and robust photosynthetic energy transfer wire. We characterized the ETE landscape by three main regions: weak localization, environment-assisted quantum transport, and strong localization, and identified the scalar $\Lambda = \frac{\lambda T}{\gamma g}$ as the key parameter to cross between these regions as one hikes over the landscape.

We showed optimality and robustness of energy transport efficiency in FMO with respect to variations in all the main external parameters dictating the dynamics. In particular, we explored the protein-solvent environment factors: system-bath coupling strength, bath memory, temperature, and spatial correlations and dissipation; the light-harvesting antenna factor: electronic state initialization; and reaction center factors: exciton trapping rate and location. Next, we investigated the performance and sensitivity of the FMO with small and large variations in its internal parameters: chromophoric spatial locations, dipole moment orientations, site energies, and chromophoric density. The exciton trapping process in FMO complex shows to be significantly robust with respect to perturbations in dipole moment orientations and site energies due to its compact structure.

We believe that a key design principle for achieving optimal and robust quantum transport performance is to allow for the convergence of energy/time scales for the contributing internal and external parameters. This phenomenon can be regarded as an examples of a Goldilocks principle in the quantum regime.

Acknowledgments

We thank A. Aspuru-Guzik, A. Ishizaki, M. Sarovar, K. B. Whaley, for useful discussions. We also thank J. H. Choi and D. Hayes for helping us with extracting the FMO data. We acknowledge funding from DARPA under the QuBE program (MM, AS, SL, HR), ENI (MM,SL), NSERC (MM) and NSF (SL, AS,HR), and ISI, NEC, Lockheed Martin, Intel (SL).

- [1] R.E. Blankenship, *Molecular Mechanism of Photosynthesis* (Blackwell Science, London, 2002).
- [2] R. K. Chain and D. I. Arnon, Proc. Natl. Acad. Sci. USA 74, 3377 (1977).
- [3] V. I. Novoderezhkin, M. A. Palacios, H. van Amerongen, R. van Grondelle, J. Phys. Chem. B **108**, 10363 (2004).
- [4] M. Cho, H.M. Vaswani, T. Brixner, J. Stenger, and G.R. Fleming, J. Phys. Chem. B **109**, 10542 (2005).
- [5] M. Grover and R. Silbey, J. Chem. Phys. **54**, 4843 (1971).
- [6] H. Haken and G. Strobl, Z. Phys. **262**, 135 (1973).
- [7] V. M. Kenkre and P. Reineker, *Exciton Dynamics in Molecular Crystals and Aggregates* (Springer, Berlin, 1982).
- [8] X. Hu, T. Ritz, A. Damjanović, and K. J. Schulten, Phys. Chem. B **101**, 3854 (1997).
- [9] T. Ritz, S. Park, and K. Schulten, J. Phys. Chem. B **105**, 8259 (2001).
- [10] W. M. Zhang, T. Meier, V. Chernyak, S. Mukamel, J. Chem. Phys. **108**, 7763 (1998).
- [11] G. D. Scholes and G. R. Fleming, *J. Phys. Chem. B* **104**, 1854 (2000).
- [12] G. D. Scholes, X. J. Jordanides, and G. R. Fleming, *J. Phys. Chem. B* **105**, 1640 (2001).
- [13] M. Yang and G. R. Fleming, Chem Phys **275**, 355 (2002).
- [14] V. May and O. Kuhn, *Charge and Energy Transfer Dynamics in Molecular Systems* (Wiley-VCH, Weinheim, 2004).
- [15] S. Jang, M.D. Newton, and R.J. Silbey, Phys. Rev. Lett. **92**, 218301 (2004).
- [16] J. Adolphs and T. Renger, Biophys. J. **91**, 2778 (2006).
- [17] T. Förster, in *Modern Quantum Chemistry, Istanbul Lectures*, edited by O. Sinanoglu (Academic, New York, 1965), Vol. 3, pp. 93–137.
- [18] G. D. Scholes, Annu. Rev. Phys. Chem. **54**, 57-87 (2003).
- [19] A.G. Redfield, Adv. Magn. Reson. **1**, 1 (1965).
- [20] G.S. Engel, T. R. Calhoun, E. L. Read, T. K. Ahn, T. Mancal, Y. C. Cheng, R. E. Blankenship and G. R. Fleming, Nature **446**, 782 (2007).
- [21] H. Lee, Y.-C. Cheng, and G.R. Fleming, Science **316**, 1462 (2007).
- [22] T. R. Calhoun, N. S. Ginsberg, G. S. Schlau-Cohen, Y.-C. Cheng, M. Ballottari, R. Bassi, and G. R. Fleming, J. Phys. Chem. B **113**, 16291 (2009).
- [23] I. Mercer, Y. El-Taha, N. Kajumba, J. Marangos, J. Tisch, M. Gabrielsen, R. Cogdell, E. Springate, and E. Turcu, Phys. Rev. Lett. **102**, 057402 (2009).
- [24] E. Collini and G. D. Scholes, Science **323**, 369 (2009).
- [25] E. Collini, C. Y. Wong, K. E. Wilk, P. M. Curmi, P. Brumer, and G. D. Scholes, Nature **463**, 644 (2010).
- [26] G. Panitchayangkoon, D. Hayes, K. A. Fransted, J. R. Caram, E. Harel, J. Wen, R. E. Blankenship, G. S. Engel, Proc. Nat. Acad. Sci **107**, 12766 (2010).
- [27] A. F. Fidler, J. R. Caram, D. Hayes, and G. S. Engel, Journal of Physics B, **45** 154013 (2012).
- [28] D. Hayes and G.S. Engel, Philosophical Transactions of the Royal Society A, **370** 3692 (2012).
- [29] M. Mohseni, P. Rebentrost, S. Lloyd, and A. Aspuru-Guzik, J. Chem. Phys. **129**, 174106 (2008).
- [30] P. Rebentrost, M. Mohseni, A. Aspuru-Guzik, J. Phys. Chem. B **113**, 9942 (2009).
- [31] P. Rebentrost, M. Mohseni, I. Kassal, S. Lloyd, and A. Aspuru-Guzik, New J. of Phys., **11**, 033003 (2009).
- [32] M.B. Plenio and S.F. Huelga, New J. Phys. **10**, 113019 (2008).
- [33] F. Caruso, A. W. Chin, A. Datta, S. F. Huelga, M. B. Plenio, J. of Chem. Phys. **131**, 105106 (2009).
- [34] A. Olaya-Castro, C. Fan Lee, F. Fassioli Olsen, and N. F. Johnson, Phys. Rev. B **78**, 085115 (2008).
- [35] A. Ishizaki and G. R. Fleming, J. Chem. Phys. **130**, 234110 (2009).
- [36] A. Ishizaki and G. R. Fleming, J. Chem. Phys. **130**, 234111 (2009).
- [37] A. Ishizaki, G.R. Fleming, Proc. Nat. Acad. Sci USA **106**, 17255 (2009).
- [38] J. Cao, R. Silbey, J. Phys. Chem. A **113**, 13826 (2009).
- [39] S. Hoyer, M. Sarovar and K. B. Whaley, New J. Phys. **12**, 065041 (2010).
- [40] F. Caruso, A. W. Chin, A. Datta, S. F. Huelga, M. B. Plenio Phys. Rev. A **81**, 062346 (2010).
- [41] M. Sarovar, A. Ishizaki, G. R. Fleming, and K. B. Whaley, Nature Physics **6**, 462 (2010).
- [42] J. Yuen-Zhou, J. Krich, M. Mohseni, A. Aspuru-Guzik, Nat. Acad. Sci USA, **108**, 17615 (2011).
- [43] S. Lloyd, M. Mohseni, New J. Phys. **12**, (2010).
- [44] D. Abasto, M. Mohseni, S. Lloyd, P. Zanardi, Phil. Trans. R. Soc. A, **3750**, 37013 (2012).
- [45] "Quantum Effects in Biology" Edited by M. Mohseni, Y. Omar, G. Engel, and M. Plenio, in preparation (Cambridge University Press, Cambridge, UK, 2013).
- [46] H. -P. Breuer and F. Petruccione, *The Theory of Open Quantum Systems* (Oxford University Press, New York, 2002).
- [47] R. Kubo, Adv. Chem. Phys. **15**, 101 (1969); Y. Tanimura and R. Kubo, J. Phys. Soc. Jpn. **58**, 101 (1989).
- [48] J. Cao, J. Chem. Phys. **107**, 8 (1997).
- [49] S. Jang, Y. Cheng, D. R. Reichman, and J. D. Eaves, J. Chem. Phys. (Communication) **129**, 101104 (2008).
- [50] Q. Shi, L. Chen, G. Nan, R. X. Xu, and Y. J. Yan, J. Chem. Phys. **130**, 084105 (2009).
- [51] A. Nazir, Phys. Rev. Lett. **103**, 146404 (2009).
- [52] P. Prior, A. W. Chin, S. F. Huelga, and M. B. Plenio, Phys. Rev. Lett. **105**, 050404 (2010).
- [53] X. T. Liang, Phys. Rev. E **82**, 051918 (2010); I. D. Vega, arXiv:1005.0465 (2010).
- [54] H. Fujisaki, Y. Zhang, and J. E. Straub, arXiv:1003.4796 (2010).
- [55] A. Shabani, M. Mohseni, H. Rabitz, S. Lloyd, Phys. Rev. E, **86** 011915 (2012).
- [56] H. Rabitz, M. Hsieh, and C. Rosenthal, Science **303**, 998 (2004); R. Chakrabarti and H. Rabitz, Intl. Rev. Phys. Chem., **26**, 671 (2007).
- [57] J. Gilmore and R. H. McKenzie, J. Phys. Chem. A, **112**, 2162 (2008).
- [58] T. Scholak, F. D. Melo, T. Wellens, F. Mintert, A. Buchleitner, arXiv:0912.3560 (2009).
- [59] EL Read, G. S. Schlau-Cohen, G. S. Engel, J. Wen, R. E. Blankenship, and G. R. Fleming, Biophys J **95**, 847 (2008).
- [60] Ying-Zhong Ma, Rebekah A. Miller, Graham R. Fleming, and Matthew B. Francis, J. Phys. Chem. B, **112**, 22 (2008).
- [61] R. A. Miller, N. Stephanopoulos, J. M. McFarland, A. S. Rosko, P. L. Geissler, and M. B. Francis, JACS (2010).
- [62] R. E. Fenna and B. W. Matthews. Nature **258** 573 (1975); B. W. Matthews, R. E. Fenna, M. C. Bolognesi, M. F. Schmid, and J. M. Olson. J. Mol. Biol. **131** 259 (1979).
- [63] Y. F. Li, W. Zhou, R. E. Blankenship, and J. P. Allen, J. Mol. Biol. **271**:456471 (1997).

- [64] In this work, whenever it is not specified otherwise, the environmental parameters for the FMO complex are chosen according to the estimated values of reorganization energy 35cm^{-1} , bath cutoff frequency 50cm^{-1} , temperature 298K , trapping rate of 1ps , exciton life-time of 1ns .
- [65] H.-P. Breuer, E. M. Laine and J. Piilo, Phys. Rev. Lett. 103, 210401 (2009).
- [66] P. Rebentrost and A. Aspuru-Guzik, arXiv:1011.3809 (2010).
- [67] J. Wu, F. Liu, Y. Shen, J. Cao, R. J. Silbey, arXiv:1008.2236.
- [68] B. Kramer and A. MacKinnon, Rep. Prog. Phys. 56, 1469 (1993).
- [69] P. Reineker and K. Kassner, J Lumin. 40, 467 (1988).
- [70] P. Castiglione, J. Phys. A: Math. Gen. 33, 1975 (2000).
- [71] I. Goychuk and P. Hänggi, Adv. Phys. 54, 525 (2005).
- [72] G. R. Fleming, M. H. Cho, Annu. Rev. Phys. Chem. 47, 109 (1996).
- [73] E. Hennebicq et al., J. Chem. Phys. 130, 214505 (2009).
- [74] F. Fassioli, A. Nazir, A. Olaya-Castro J. Phys. Chem. Lett., 1, 2139 (2010).
- [75] M. Sarovar, Y. Cheng, K. B. Whaley, Phys. Rev. E, 83, 011906 (2011).
- [76] A. Ishizaki, T. R. Calhoun, G. S. Schlau-Cohen, and G. R. Fleming, Phys. Chem. Chem. Phys. 12, 7319 (2010).
- [77] N. Demirdöven, M. Khalil and A. Tokmakoff, Phys. Rev. Lett., 89, 237401.125 (2002); M. Khalil, N. Demirdöven and A. Tokmakoff, J. Phys. Chem. A, 107, 5258 (2003).
- [78] C. Olbrich, J. Strümpfer, K. Schulten, U. Kleinekathöfer, J. Phys. Chem. B, 115, 758 (2011).
- [79] D.A. Lidar, I.L. Chuang, K.B. Whaley, Phys. Rev. Lett. 81, 2594 (1998); M. Mohseni, J. S. Lundeen, K. J. Resch, A. M. Steinberg, Phys. Rev. Lett. 91, 187903 (2003) A. Shabani, D.A. Lidar, Phys. Rev. A 72, 042303 (2005).
- [80] Remigy, H. W., H. Stahlberg, D. Fotiadis, B. Wolpensinger, A. Engel, G. Hauska, and G. Tsiotis, J. Mol. Biol. 290, 851 (1999).
- [81] J. Wen, H. Zhang, M. L. Gross, R. E. Blankenship, Proc. Natl. Acad. Sci. USA 106, 6134 (2009).
- [82] M.K. Sener, D. Lu, T. Ritz, S. Park, P. Fromme, and K. Schulten, J. Phys. Chem. B 106, 7948 (2002).
- [83] S. Lloyd, lecture at Santa Fe Institute, 1990, as reported by Murray Gell-Mann, "The Quark and the Jaguar".
- [84] The FMO PDB file was provided by M. Cho laboratory.

Appendix A: FMO free Hamiltonian

In this work we use the following free Hamiltonian for the FMO complex, given in Ref. [4]:

$$H = \begin{pmatrix} 280 & -106 & 8 & -5 & 6 & -8 & -4 \\ -106 & 420 & 28 & 6 & 2 & 13 & 1 \\ 8 & 28 & 0 & -62 & -1 & -9 & 17 \\ -5 & 6 & -62 & 175 & -70 & -19 & -57 \\ 6 & 2 & -1 & -70 & 320 & 40 & -2 \\ -8 & 13 & -9 & -19 & 40 & 360 & 32 \\ -4 & 1 & 17 & -57 & -2 & 32 & 260 \end{pmatrix}$$

The estimated values of dipole moment orientations and positions of the Mg atoms, representing the location of Bchls, are extracted from the pdb file of the FMO complex [84]. These data can be summarized in the following table:

The Bchl-Bchl coupling in FMO is dipole-dipole interac-

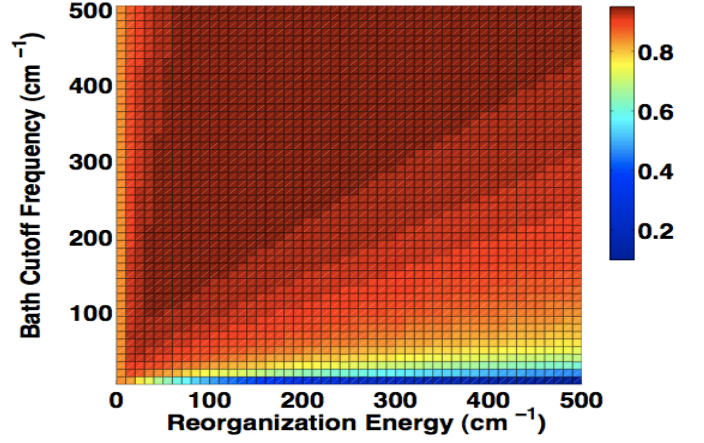


FIG. 18: The top view of FMO energy transfer landscape in the presence of an Ohmic model of bath spectral density as a function of reorganization energy and bath frequency cutoff at room temperature. The ETE predicted by this model is below the estimate values by a Lorentzian model and therefore it cannot explain near ideal performance of FMO complex in exciton transport. Nevertheless, here we can also observe the three distinct regimes of weak and strong localizations close to γ and λ axes, and the intermediate optimal ENAQT, separated by straight lines. This plot confirms the role of parameter $\lambda T/\gamma$ as an effective governing parameter.

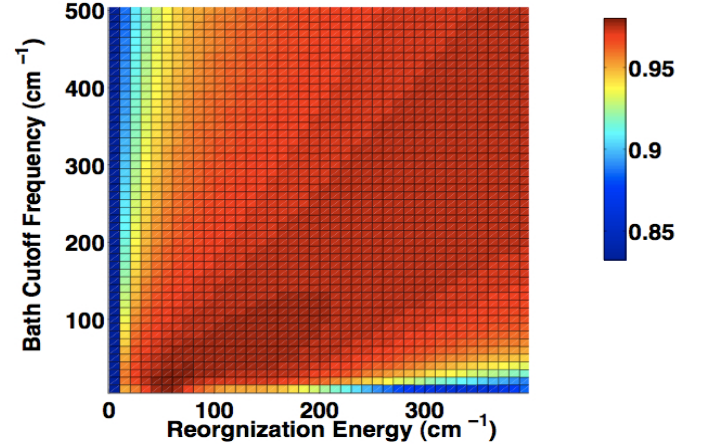


FIG. 19: Top view of the ETE landscape at 77°K for a bath with a Lorentzian spectral density. The general pattern of an optimal transport region in between two limits of localized low-efficient transport regimes, divided by rather straight lines, is observed here as well. However, due to low-temperature effects captured in the parameter $\lambda T/\gamma$, the adversarial high reorganization and slow bath effects become less pronounced leading to a higher ETE than those in Fig. 3 in the corresponding limits.

tion

$$J_{jk} = \frac{C}{R_{jk}^3}(\mu_j \cdot \mu_k - \frac{3}{R_{jk}^2}(\mu_j \cdot \mathbf{R}_{jk})(\mu_k \cdot \mathbf{R}_{jk})), \quad (\text{A1})$$

for which we choose the constant $C|\mu|^2 = 134000\text{cm}^{-1}\text{\AA}^3$ [16].

TABLE I: Spatial location of Bchls and their dipole moment orientation.

Bchl	x (Å)	y (Å)	z (Å)	θ	ϕ
1	28.032	163.534	94.400	0.3816	-0.6423+ π
2	17.140	168.057	100.162	0.067	0.5209+ π
3	5.409	180.553	97.621	0.1399	1.3616+ π
4	9.062	187.635	89.474	0.257	-0.6098+ π
5	21.823	185.260	84.721	-0.1606	0.6899+ π
6	23.815	173.888	82.810	-0.4214	-1.4686+ π
7	12.735	174.887	89.044	0.578	-1.0076+ π

Appendix B: Energy transfer efficiency for Ohmic bath and cryogenic temperature

Here, we demonstrate that separation of ETE landscape, as a function of the parameter $\lambda T/\gamma$, into the various regions with distinct quantum transport efficiencies is not a mere prop-

erty of either Lorentzian bath or high temperature limit. A top view of FMO energy transfer landscape is shown for an Ohmic spectral density at 298°K and Lorentzian spectral density at 77°K in Fig. 18 and Fig. 19 respectively. In each figure, one can distinguish three different regions including low-efficient weakly localized limit, optimal EANQT, and low-efficient strongly localized limit, similar to the results presented in Fig. 3.

It should be noted that a bath with an Ohmic regularized spectral density, $J(\omega) = \lambda(\omega/\gamma) \exp(-\omega/\gamma)$, has often been employed in modeling the effect of bath fluctuations on the spectroscopic readout of an FMO sample [4, 72]. Figure 18 presents the top view ETE landscape as a function of bath reorganization energy and cutoff frequency with an Ohmic density. The observed high efficient region stays lower than its Lorentzian counterpart in Fig. 3, therefore is unable to explain the high efficiency of the FMO complex. This can be seen as a confirmation for the theoretical modeling of the solvent-protein environment with Lorentzian spectral densities [57].